Metered Dose Inhaler Aerosols:

Efficiency, Particle Engineering and

Atomization

By

Farzin Molaghasem Shemirani

A thesis submitted in partial fulfillment of the requirements for the degree
of
Doctor of Philosophy

Department of Mechanical Engineering

University of Alberta

Abstract

The current work focuses on three different aspects of the aerosols involved in Metered Dose Inhaler (MDI) sprays. The efficiency of the drug delivery in different ambient conditions, production of monodisperse solid particles to study the heat and mass transfer processes involved, and study of flash atomization process in a propellant jet are the main topics in the present work.

The aim of the first part is to investigate *in vitro* mouth-throat deposition and lung delivery of selected solution and suspension pMDI formulations, under a range of relative humidity, temperature and flow rate conditions. The Alberta Idealized Throat was connected to a collection filter, and placed in an environmental control chamber. The formulations selected were beclomethasone dipropionate (BDP) in 13% w/w ethanol/1.3% w/w glycerol and HFA134a propellant solution ('BDP HFA134a'), BDP in 13% w/w ethanol and HFA227 propellant solution ('BDP HFA227'), and Flixotide Evohaler (fluticasone propionate 250 µg/dose in HFA134a suspension). Each of these pMDI formulations were dispersed into the mouth-throat and filter assembly in triplicate, according to an experimental matrix consisting of the following conditions – air flow rates of 28.3, 60 and 90 L/min; 0%, 35% and 80% RH; operating temperatures of 20°C and 40°C. There was a general increase in mouth-throat deposition, and corresponding decrease in filter deposition (representing lung dose fraction), with increasing relative humidity for both BDP HFA134a and Flixotide pMDIs. Increasing temperature from 20 to 40°C resulted in decreased mouth-throat deposition and

increased lung dose fraction for the solution pMDIs, but generally no effect for the suspension pMDI. Not only is the dose delivery of pMDI formulations affected by environmental conditions (in some cases causing up to 50% reduction in lung delivery), but solution and suspension formulations also behave differently in response to these conditions. These results have implications for dosage form design and testing, and for patient use.

The second part describes an atomizer capable of generating monodisperse droplets of high vapor pressure liquids such as HFA227ea and HFA134a, which is expected to be a useful tool in future fundamental explorations of the mechanics of these highly dynamic aerosols. Hydrofluoroalkanes (HFAs) are the most common propellants in metered dose inhalers (MDIs), which are themselves the most common delivery method for pulmonary disease medications. As a result of the high vapor pressure of these fluids, generation of monodisperse droplets and their study are not possible with previously existing monodisperse atomizers due to fluid flashing when exposed to ambient conditions. The new atomizer uses a piezoelectric transducer to disintegrate the propellant jet, a cooling circuit with a low temperature limit of $-30\ °C$ to reduce propellant vapor pressure, and a high pressure feed system (up to 2.7 MPa) to keep the propellant in the liquid phase, thereby avoiding flash atomization. In the current setup, the diameter of the generated droplets was monitored with a laser scattering system (using Fraunhofer diffraction theory) to optimize the operating parameters of the set-up (for example, the actuation frequency and amplitude of the piezoelectric transducer).

This monitoring system allowed for the measurement of droplet geometric diameter, spacing, and velocity. The capabilities of the atomizer for generating monodisperse droplets are demonstrated by a case study in which monodisperse dry particles of beclomethasone dipropionate (BDP) are generated using a solution of BDP, ethanol co-solvent, and HFA134a propellant.

The parameters affecting the onset of flash atomization in cylindrical micro-jets were studied in the third part. A custom atomizer, a pressurized feed system, and a controlled flow tube were designed to produce stable jets of propellant mixtures at different initial liquid temperatures. Propellants chosen were HFA134a and HFA227ea which are used in most pressurized metered dose inhalers (MDIs). Ethanol, a common co-solvent in MDIs, was also added to the propellants at 10, 15 and 20% w/w concentrations to investigate its effect on flashing. Orifices used for the production of the jets ranged from 5 to 35 μm in diameter. A critical jet diameter above which flashing was the dominant mechanism of atomization was found at each temperature and formulation. A correlation was developed to relate the critical jet diameter to the thermo-physical properties of the formulation at different temperatures.

Preface

This thesis is an original work by Farzin Molaghasem Shemirani. Chapter 2 of this thesis has been published as: Shemirani, F. M., Hoe, S., Lewis, D. Church, T., Vehring, R., Finlay, W. H. "In-vitro investigation of the effect of ambient humidity on regional delivered dose with solution and suspension MDIs", J. Aerosol Med. Pulm. Drug. Del., 26: 215-222, 2013. I was responsible for designing and assembling the experimental setup as well as taking the tests and writing the manuscript. Susan Hoe assisted in running the tests and writing the manuscript. David Lewis, Tanya Church, Reinhard Vehring, and Warren Finlay acted as supervisors of the project.

Chapter 3 of this thesis has been submitted to Journal of Atomization and Sprays as: Mehdi Azhdarzadeh, Farzin M. Shemirani, Conor A. Ruzycki, Alberto Baldelli, James Ivey, David Barona, Tanya Church, David Lewis, Jason S. Olfert, Warren H. Finlay, and Reinhard Vehring "An atomizer to generate monodisperse droplets from high vapor pressure liquids". I was responsible for designing, manufacturing and testing of the experimental setup and data analysis as well as assisting in writing the manuscript. Mehdi Azhdarzadeh assisted in design of the atomizer and the manuscript composition. Conor A. Ruzycki contributed in taking the tests. James Ivey assisted in discussing the data. Alberto Baldelli helped in setting up the test rig. David Barona assisted in manuscript writing as well as building the experimental setup. All the other authors shared the supervision of the project.

Chapter 4 of this thesis has been submitted to International Journal of Multiphase Flow as: Farzin M. Shemirani, Tanya K. Church, David A. Lewis, Warren H. Finlay, Reinhard Vehring as: "Onset of flash atomization in a propellant micro-jet". I was responsible for design of the experiment, running the tests, and composition of the manuscript. Tanya Church, David Lewis, Warren Finlay and Reinhard Vehring served as supervisors of the work.

Dedication

I would like to dedicate this work to my brother Farzad,

who never hesitated in helping me when I needed him

most.

Acknowledgements

Table of Contents

List of Tables

List of Figures

Chapter 1. Introduction

1.1 INTRODUCTION TO METERED DOSE INHALERS

Pressurized metered dose inhalers (pMDI or MDI) are widely used in pulmonary drug delivery. Compared to other inhalers (dry powder inhalers and nebulizers) they are more popular because of being relatively inexpensive and because of their ease of use [1, 2]. Essential components of a metered dose inhaler are shown schematically in Figure 1-1. As it can be seen from Figure 1-1 formulation (1) is kept inside a container (6) which itself is seated inside the actuator (4). The metering valve (3) holds a known amount of the mixture (typically between 25 µL and 100 µL [3]) ready to be released and provide nearly 50-250 µg of drug [4]. The main purpose of having the metering valve is to deliver a reproducible amount of drug to the patient.

By depressing the canister inside the actuator, the valve stem (2) slides through the metering valve and pressurized formulation passes through the valve stem, actuator sump (7) and actuator orifice (8).
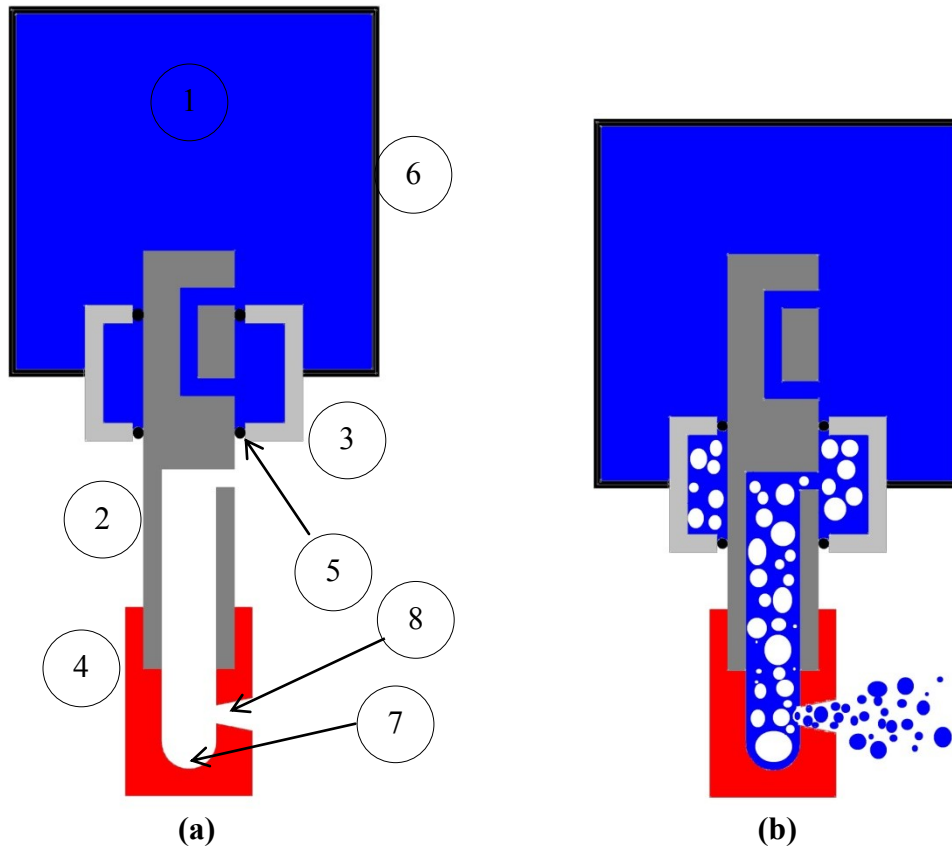
Figure 1-1 **(a)** Schematic of the basic components of a metered dose inhaler prior to actuation: (1) formulation inside the canister, (2) valve stem, (3) metering volume, (4) actuator, (5) gaskets, (6) container, (7) sump, (8) actuator orifice, **(b)** Schematic of an MDI spray after actuation, adapted from Ivey et al. [5]

After depressurization, the stationary liquid rapidly turns into a two-phase flashing flow to reach thermodynamic equilibrium at atmospheric pressure [6]. After the MDI is actuated and the formulation is released, a spring returns the valve stem to its original position and the metering valve is refilled because of the gravity, ready for the next shot.

2

1.1.1 Container

The container can be aluminum or glass. Aluminum containers are compact, lighter than glass vials and light proof. Glass containers are inert and transparent that makes them favorable when one desires to know the vial content [4]. When glass containers are used, they should be plastic-coated or laminated to be able to handle high vapor pressures of the formulation inside the container. Typically, they are required to handle a pressure of 1.2 MPa [7, 8]. Both aluminum and glass containers should also be coated to avoid adhesion of drug or chemical degradation [9].

1.1.2 Actuator

The actuator is a plastic housing used for holding the container. It includes a barrel like structure that surrounds the container, a sump, actuator orifice, and the mouth piece as shown in Figure 1-1. It is generally made from polypropylene [10]. The actuator orifice is an integral part of the MDI design which contributes to control of droplet size distribution released from pMDIs. The diameter of the actuator orifice ranges from 0.14 mm to 0.6 mm [9]. The lengths of the actuator sump and actuator orifice have been proven to affect spray pattern, particle size distribution, and plume temperature of MDIs [11, 12].

1.1.3 Gaskets

Gaskets (Figure 1-1) or elastomers are a necessary part of the MDI hardware. They should be chemically compatible with the formulation to keep the concentration of extractables low in the formulation [9]. Typical gaskets used with HFA containing formulations are: nitrile, ethylene-propylene-diene monomer (EPDM), and chloroprene [4].

1.1.4 Formulation

The formulation used in MDIs can be either solution or suspension. Either types contain the propellant agent that can be HFA134a, HFA227ea or CFCs[1] (or a combination of them), active pharmaceutical ingredient and excipients. Suspension MDIs contain micron-sized drug particles suspended in the propellant, while in solution MDIs the drug is dissolved in the propellant using a co-solvent[2] [4]. A short list of the drugs used in commercial HFA MDIs is tabulated in Table 1-1.

---

[1] Because of their ozone depletion potential CFCs are in the process of phasing out.

[2] Co-solvents may serve to increase the solubility of the excipients as well.

Table 1-1 A list of the drugs used in commercial metered dose inhalers and their manufacturers [4, 13-15]

Active pharmaceutical ingredient	Brand name	Manufacturer
Salbutamol	Airomir®	3M
	Ventolin Evohaler®	Allen & Hanburys
Beclomethasone dipropionate	Qvar®	3M
	Clenil® Modulite®	Chiesi
	Fostair	Chiesi
Fluticasone	Evohaler	Allen & Hanburys
Ciclesonide	Alvesco®	Nycomed
Fluticasone propionate	Flixotide® Evohaler®	GlaxoSmithKline
Formoterol, budesonide	Symbicort®	AstraZeneca

Some well-known excipients used are: ethanol, water, glycerin, oleic acid, and menthol. Each of these excipients have its own functionality; for instance, ethanol is being used to solubilize drug in the propellant while oleic acid is being used as dispersive agent [16].

Basic thermo-physical and environmental properties of HFA134a and HFA227ea are listed in Table 1-2. As it is seen in the table, both HFAs have relatively high vapor pressures at room temperature. That is the reason they should be kept pressurized in the canister to keep them in the liquid phase.

HFA propellants are not ozone depleting agents, but they have high global warming potentials. That is why the search for new propellants is ongoing and two suggested ones having low global warming effect are trans-1,3,3,3,-tetrafluoropropene (HFO-1234ze) and 2,3,3,3,-tetrafluoropropene (HFO-1234yf) [16]. They have similar thermo-physical properties to the current HFA propellants, but more research needs to be done before using them in commercial MDIs.

1.1.5 MDI spray

High vapor pressure of the propellant mixture leads to generation of a high velocity spray out of the MDI actuator orifice and disintegration of the liquid propellant to fine respirable-sized droplets. The expanded spray contains millions of highly volatile droplets and lasts nearly 0.1-0.5 s [12, 17]. Velocity of the HFA pMDI sprays has been reported to be nearly 30 m/s at the mouthpiece and between 2.0 and 8.4 m/s at 10 cm distance from the nozzle [12, 18].

The MDI plume is a highly turbulent, two-phase flow and is transient which makes it quite complicated to study. A detailed visual study by Versteeg and Hargrave [19] on the MDI spray has proved the highly transient nature of the process.

After the atomization process droplets continue to evaporate and cool down because of losing the latent heat of evaporation to the point when they reach their lowest

temperature, which is called wet bulb temperature[1]. Droplets continue to lose their mass

until only the non-volatile content of the formulation remains in the droplet. The

number of residual particles of MDIs has been estimated to be up to 300 million

particles [20]. In case of solution MDIs, the number of residual particles and the number

of produced droplets are identical, but in suspension MDIs the number of residual

particles is much lower than the number of produced droplets because some of the

droplets do not contain any drug particles while others contain multiple ones [21].

The size of the residual particles of MDI spray for solution systems has been shown to

be only a function of the choice of the propellant and the concentration of non-volatile

content of the formulation (NVC) as follows [22]:

$$MMAD_{HFA134a} = 2.31 \ \%NVC^{\frac{1}{3}} \hspace{4cm} (1\text{-}1)$$

$$MMAD_{HFA227ea} = 3.2 \ \%NVC^{\frac{1}{3}} \hspace{4cm} (1\text{-}2)$$

In equations (1-1) and (1-2), MMAD is the mass median aerodynamic diameter. The

aerodynamic diameter is the diameter of a unit density sphere that has the same settling

---

[1] MDI spray affects and is affected by the ambient conditions, . for example, the temperature of the air

affects the evaporation process of the droplets and evaporation of the droplets cools down the air

temperature around the spray.

velocity in air as the particle of interest. The mass median aerodynamic diameter of a particle size distribution is the aerodynamic diameter at 50% of the cumulative mass distribution [23].

Previous studies have been carried out to estimate the MMAD of the residual particles released from suspension MDIs having HFA134a propellant, and the proposed correlations are as follows [24]:

$$MMAD_R = 0.768 \left(MMAD_{Drug}\right) + 0.0759(MMD_I) + 88.6 \left(C_{Drug}\right) + \frac{7.25\left(C_{Drug}\right)}{MMAD_{Drug}^3} - 0.4 \quad (1\text{-}3)$$

$$MMD_I = 6.90 + 0.0441(VS) + 23.6(C_{EtOH}) - 63.8(C_{EtOH})^2 + 24.7(C_{EtOH} \times OD) \\ - 0.129(C_{EtOH} \times VS) \quad (1\text{-}4)$$

In above equations $MMAD_R$ is the MMAD of residual particles released from an HFA134a suspension MDI in (μm), $MMAD_{Drug}$ is the MMAD of the suspended drug particles in (μm), MMD_I is the mass median diameter of the initial droplets (μm), C_{Drug} is the mass fraction of the drug particles in the formulation, VS is the volume of the metering valve in (μL), C_{EtOH} is the mass fraction of the ethanol in the formulation, and OD is actuator orifice diameter in (mm).

Residual particles having MMAD between 0.5 and 5 μm are favorable for drug delivery to the lung [24]. Particles larger than this range have the tendency to deposit in the oropharyngeal region due to inertial impaction (see sections 1.2.1 and 1.2.4).

Table 1-2 Thermo-physical and environmental properties of HFA134a and HFA227ea [16, 25, 26]

	HFA134a	HFA227ea
Molecular formula	$C_2H_2F_4$	C_3HF_7
Chemical name	1,1,1,2-Tetrafluoroethane	1,1,1,2,3,3,3-Heptafluoropropane
Molecular weight	102.0	170.0
Ozone Depletion Potential	0	0
Global Warming Potential°	1300	2900
Atmospheric Life (years)	14.6	36.5
Boiling Point at 1.1013 kPa [°C]	−26.3	−16.5
Freezing Point [°C]	−101	−131
Critical temperature [°C]	101.15	101.09
Critical pressure [bar]	40.64	29.52
Critical density $\left[\frac{kg}{m^3}\right]$	507	592
Vapor pressure [bar]*	5.72	3.9
Liquid density $\left[\frac{kg}{m^3}\right]$*	1226	1408
Saturated vapor density $\left[\frac{kg}{m^3}\right]$*	28	31
Specific heat capacity of the liquid $\left[\frac{J}{kg.K}\right]$*	1402	1148
Liquid thermal conductivity $\left[\frac{mW}{m.K}\right]$*	85.7	59.45
Liquid-vapor surface tension $\left[\frac{mN}{m}\right]$*	8.69	6.96

°Based on 100-year global warming potential compared to that of CO_2
*at 20 °C

1.2 EFFECT OF AMBIENT CONDITIONS

Chapter two focuses on the effect of ambient conditions on the regional deposition of MDI sprays. Orally inhaled aerosols must first pass through the extrathoracic region before reaching the lung. The extrathoracic region includes: oral cavity (or buccal cavity), oropharynx (throat region between the larynx and the moth) and larynx (a constriction just before the trachea) [27]. The most important aerosol deposition mechanism in the extrathoracic region, or simply mouth-throat, is inertial impaction[1] (see section 1.2.1).

The carrier gas properties affect aerosol deposition in the airways too. It has long been known that gas temperature, humidity, flow rate, and density can affect inhalers performance. These properties are more studied in the cases of intubated patients where carrier gas (air) should be warm and humid in order not to damage the mucus [28]. It is believed that heated humid air can reduce the amount of drug delivered to the lung by up to 40% [29].

---

[1] Other deposition mechanisms are gravitational sedimentation and diffusion, both not important in extrathoracic deposition compared to inertial impaction.

1.2.1 Inertial impaction

Inertial impaction occurs when the particle/droplet does not follow the gas flow streamline at the bends and impacts to the walls of airways. The parameter defining the relative importance of the inertial impaction is a dimensionless group called Stokes number as defined below:

$$Stk = \frac{U_0 \rho_{\text{particle}} d^2 C_c}{18 \mu D} \tag{1-5}$$

Where U_0 is the characteristic gas velocity, ρ_{particle} is the density of the particle, d is the diameter of the particle, C_c is the Cunningham correction factor, μ is the viscosity of the gas, and D is the characteristic length scale of the airway. Particles/droplets having high Stk numbers tend to deposit more in the mouth-throat while ones having lower Stk numbers pass through the trachea and lung. Although equation (1-5) looks simple to use, it has many details that should be taken care of. Those details are listed in Table 1-3.

Table 1-3 Issues in defining the stokes number for aerosols [27, 30]

Parameter	Issue
U_0	Defining a single characteristic velocity is not an easy task because the geometry and dimensions of the extrathoracic region varies at each section, from person to person, and is inhalation flow rate dependent.
$\rho_{particle}$	Particles are not always perfect solid homogenous spheres. They can have internal pores that give them lower densities.
d	It is hard to define a geometric diameter for non-spherical particles and many definitions exist. Even spherical particles can have surface structures that should be counted for when defining the diameter. Diameter definition is important in defining the density of the particle, $\rho_{particle}$, too.
C_c	It accounts for cases where assumption of gas phase continuum is not valid.
D	Similar to the issue for U_0, it is hard to define a characteristic length scale.

1.2.2 Temperature

Air temperature can affect in different ways. Droplets produced by metered dose inhalers evaporate faster at higher temperatures. Higher evaporation rate results in existence of finer droplets (or even solid residual particles) in the oropharyngeal region which consequently decreases impaction rate.

At higher temperatures, vapor pressure of the HFA propellants increases rapdily (HFA134a undergoes 78% increase in its vapor pressure when the temperature changes

from 20°C to 40°C, HFA227ea's vapor pressure increase 80% at the same conditions [25, 26]).

Since a major factor in the atomization process of the MDI is flash evaporation in the expansion chamber [31], higher vapor pressure may lead to having a more intense flash evaporation and a change in the size of the initial droplets emitted from the actuator orifice.

Another effect can be due to changes in the mass of the formulation contained in the metering volume. At higher temperatures, the formulation has a lower density. This leads to the existence of reduced drug mass in the metering volume and, therefore, reduction in the dose emitted from the MDI.

1.2.3 Humidity

As the volatile HFA droplets of MDI evaporate, they reach a final low temperature called "wet bulb temperature". For HFA134a and HFA227ea droplets, this final temperature is quite low. The wet bulb temperature of HFA134a droplets has been estimated to be around -64°C [27]. This low temperature makes the residual solid particle of the MDI a potential nucleus for condensation of water vapor and condensational growth. An increase in the diameter of the droplets/particles because of this growth increases the value of the Stokes number (equation (1-5)) and the possibility of inertial impaction of the particles to airway walls. Humidity has been shown to have

no effect on the evaporation rate of HFA droplets (specifically HFA227ea droplets with and without ethanol) [32].

1.2.4 Inhalation flow rate

As it was seen in section 1.2.1, the carrier gas velocity plays an important role in inertial impaction. Numerous studies have been carried out to show the importance of the inhalation flow rate on oropharyngeal deposition of orally inhaled aerosols [33-36]. This effect has been quantified in two ways: impaction parameter, $d_a^2 Q$ and deposition parameter, $Stk^\alpha Re^\beta$; d_a is the aerodynamic diameter, Q is the volumetric flow rate, Stk is the Stokes number, and Re is the Reynolds number of the gas flow in the airway. All the studies have shown that for orally inhaled aerosols an increase of flow rate increases the inertial impaction deposition rate in the extrathoracic region. Such a trend has not been observed for inhalation of MDI aerosols; even it has been observed that higher inhalation flow rates leads to lower mouth-throat deposition [37]. This observation in case of MDI spray has been attributed to the effect of turbulent mixing happening in the oral cavity due to the difference between MDI plume velocity and air velocity. The higher the difference between the two, the higher is the deposition due to turbulent mixing.

1.3 PRODUCTION OF MONODISPERSE PROPELLANT DROPLETS

A wide range of droplet sizes exists in the MDI spray. The residual particle size distribution of MDIs has been reported to have geometric standard deviations (GSD) between 1.61 and 2.14[1] [38]. This wide droplet size distribution as well as the very transient nature of the process makes the study of the heat and mass transfer processes happening in individual droplets quite complicated. To overcome this issue, in Chapter three, the design of a novel atomizer assembly to produce monodisperse droplets of propellant formulations has been explained. The motivation to the design is to facilitate the study and engineering of individual particles produced by MDIs.

To produce monodisperse droplets of HFA propellant mixtures, Rayleigh disintegration theory of cylindrical jets was employed. Rayleigh theory predicts that cylindrical liquid jets are unstable to disturbances having wavelengths larger than the circumference of the jet [39]. This theory has been previously employed by many researchers to produce

---

[1] Geometric standard deviation of a particle/droplet size distribution is defined as the standard deviation of the logarithm of the particle/droplet diameters. It can be approximated as $GSD = (d_{84}/d_{16})^{0.5}$, where d_{84} and d_{16} are the diameters at which 84% and 16% of the particles/droplets total mass is due to the particles smaller than those diameters, respectively. Larger GSD means wider particle size distribution. (Finlay 2001)

monodisperse droplets of non-volatile liquids but not for highly volatile ones [40-43].

To be able to produce monodisperse droplets, the jet breakup regime should be in the

Rayleigh breakup region (see section 1.3.1).

1.3.1 Liquid jet breakup regimes

A comprehensive study on liquid jet breakup regimes has been carried out by Reitz

[44]. According to Reitz a liquid jet in air undergoes different types of stresses; surface

normal stress, shear stress, and inertial stress. These stresses contribute to disintegration

or breakup of the jet. Jet breakup regimes have been categorized to be: dripping regime,

Rayleigh regime, first wind-induced regime, and second wind-induced regime[1]. The

dripping regime happens when the jet velocity is so low that jet itself is not formed [45].

The Rayleigh region happens when the jet is formed but breaks up due to radially

symmetric waves introduced by mechanical disturbances[39]. The first wind-induced

regime happens when aerodynamic forces of the air are not negligible anymore and

surface waves are axisymmetric. In this region the size of the droplets produced are still

of the same order as the jet diameter [39, 45]. In the second wind-induced regime, the

effect of aerodynamic forces on the jet breakup is dominant and the droplets produced

---

[1] Another mode of jet breakup is the atomization regime happening in subcooled liquids. In which the
disintegration starts at nozzle exit. This mode is similar to second-wind induced regime as it is still wind-
induced. In this mode very fine droplets are produced (Lin and Reitz 1998).

are much smaller than the diameter of the jet [46]. Knowing that Reynolds, Weber, and Ohnesorge dimensionless numbers represent the ratio between the different stresses applied to the jet, one can categorize different jet disintegration modes using these numbers. The summary of jet breakup regimes is listed in Table 1-4.

Table 1-4 Different breakup regimes of a cylindrical liquid jet in a gas phase [45, 46]

Breakup regime	criteria	Note
Dripping regime	$We_{\mathrm{L}} < 8$	Balance between liquid inertia force and surface tension force
Rayleigh regime	$We_{\mathrm{L}} > 8$	Balance between liquid inertia force and surface tension force
	$We_{\mathrm{g}} < 0.4$	Gas inertia force equals 10% of surface tension force
	$We_{\mathrm{g}} < 1.2 + 3.41 Oh^{0.9}$	Corresponds to maximum jet breakup length
First wind-induced regime	$We_{\mathrm{g}} < 13$	Upper end corresponds to the point where gas inertia force is of the same order as surface tension force
Second wind-induced regime	$13 < We_{\mathrm{g}} < 40.3$	Upper end corresponds to onset of atomization regime

Definitions of dimensionless numbers used in Table 1-4 are as follows:

$$We_{\text{L}} = \frac{\rho_{\text{L}} U_{\text{L}}^2 d}{\sigma} \tag{1-6}$$

$$We_{\text{g}} = \frac{\rho_{\text{g}} U_{\text{L}}^2 d}{\sigma} \tag{1-7}$$

$$Oh = \frac{\mu_{\text{L}}}{\sqrt{\rho_{\text{L}} d \sigma}} \tag{1-8}$$

In equations (1-6), (1-7), and (1-8), ρ_{L} is the liquid density, ρ_{g} is the gas density, U_{L} is the jet velocity, d is the jet diameter, σ is the liquid-vapor surface tension and μ_{L} is the liquid viscosity.

1.4 FLASH ATOMIZATION

In classical thermodynamics, the liquid-vapour phase change process is treated as a process happening through thermal equilibrium. However, in practical cases, processes could be fast enough that the liquid and vapour does not have enough time to reach thermal equilibrium during the phase change. This non-equilibrium process can happen in two different ways: heating of the liquid and rapid pressure reduction of the container. The former is called boiling, and the latter is called flashing [47].

During the liquid-vapour phase change process, bubbles can appear within the liquid phase or at the liquid-solid interfaces. When the bubbles form everywhere within the liquid phase, homogeneous nucleation is happening, and when they form at the

interfaces heterogeneous nucleation is happening. In case of homogeneous nucleation, bubbles form because of the local fluctuations of the density, but in heterogeneous nucleation, bubbles already exist (or are trapped) inside the scratches on the container walls [48].For both nucleation types to occur, the temperature of the liquid phase needs to be higher than the saturation temperature of the liquid (corresponding to liquid pressure). The difference between these two temperatures is called degree of superheat. It is known that homogeneous nucleation needs a much higher degree of superheat to occur (superheat limit) than heterogeneous nucleation [49, 50].

Flashing can also happen in a metastable liquid, which is a liquid not in thermal or mechanical equilibrium with its vapor and which did not have enough time for the bubbles to grow and reach equilibrium. It is known that passing of the liquid through an orifice with downstream pressures below the saturation pressure (corresponding to the liquid temperature) leads to the metastable liquid phase [51].

Flashing can happen in the liquid jets too which is called flash atomization. Flash atomization in jets is defined as the disintegration or shattering of a metastable liquid jet due to the rapid growth of vapor bubbles [52].

In chapter four, the occurrence of flash atomization in micro-jets of mixtures containing HFA134a and HFA227ea was controlled through manipulation of jet diameter, upstream jet temperature, and formulation. Doing so, it is possible to have a better understanding of the effect of different thermo-physical properties on onset of flash atomization in micro-jets.

Chapter 2.   In-vitro investigation of the effect of ambient humidity on regional delivered dose with solution and suspension MDIsIn-vitro investigation of the effect of ambient humidity on regional delivered dose with solution and suspension MDIs[1]

2.1 INTRODUCTION

Although inhaler studies are often conducted in controlled laboratory conditions, at the patient end inhalers are stored and used in a wide variety of temperatures and

---

[1] This chapter has been published as: Shemirani, F. M., Hoe, S., Lewis, D. Church, T., Vehring, R., Finlay, W. H. "In-vitro investigation of the effect of ambient humidity on regional delivered dose with solution and suspension MDIs", J. Aerosol Med. Pulm. Drug. Del., 26: 215-222, 2013. Farzin M. Shemirani was responsible for designing and assembling the experimental setup as well as taking the tests and writing the manuscript. Susan Hoe assisted in running the tests and writing the manuscript. David Lewis, Tanya Church, Reinhard Vehring, and Warren Finlay acted as supervisors of the project.

humidities. The effect, if any, of temperature and humidity on the dose delivery into the respiratory tract, is a factor that may need considering when predicting the behaviour of medical aerosols under realistic patient use conditions.

Dose delivery into the lung has been estimated *in vitro* based on particle size distributions of an aerosol created by a pressurized metered dose inhaler (pMDI). Cascade impactors are used to measure the diameter of the aerosol particles after propellant evaporation, while laser diffraction techniques are usually employed to measure droplet diameter within the pMDI aerosol plume. The general assumption is that larger particles are more likely to deposit in the mouth and throat, reducing lung deposition. Hence, the effect of temperature and humidity on droplet diameter has been employed as a predictor for the delivery of pMDI formulations in varying environmental conditions [53, 54].

Many studies investigating particle diameter changes with variation in relative humidity have used *in vitro* models representing mechanical ventilation for intubated patients, where a humidifier is used to deliver nebulized solutions or pMDI formulations via a spacer. Ari *et al.* found that post-endotracheal tube delivery of the commercial pMDI ProAir (108µg salbutamol sulphate per dose) was lower in a heated and humidified circuit, compared to one that was not [55]. Lin *et al.* used a similar setup (replacing ProAir with another salbutamol sulphate pMDI), and reported that the total inhaled drug mass decreased from 23 ± 2.1 to $11.4 \pm 3.8\%$ after 2 hours of circulation in 37°C/100% RH conditions [56].

Lange and Finlay, employing an *in vitro* model for mechanically ventilated pediatric patients, suggested that mole fraction of water vapour in air, rather than relative humidity, was a more relevant parameter for investigating droplet evaporation. When the mole fraction was kept constant in dry air, an increased air temperature (25, 30 and 37°C) resulted in increased post-endotracheal tube (ETT) deposition of salbutamol sulfate (100μg/dose in CFC); increased propellant evaporation at higher temperature was the authors' proposed explanation. A decrease in post-ETT deposition was observed with increasing mole fraction. At 37°C, $19.1 \pm 2.1\%$ was deposited for a mole fraction of 0.058 (equivalent to 100% RH), compared to $41.1 \pm 1.2\%$ for a mole fraction of 0.005 (equivalent to 8% RH). Lange and Finlay hypothesized a decreased propellant evaporation rate, due to reduced propellant vapour pressure at high water vapour mole fraction [57].

However, data presented by Martin *et al*. does not support this hypothesis. The evaporation rate of single, pendant, HFA227-only propellant droplets in dry (37°C < 10% RH) and humid (37°C /100% RH) air, was calculated from the visual observation of change in droplet volume over time. No significant difference was found in propellant evaporation rates between dry and humid conditioned air [58].

Martin and Finlay observed that two commercial salbutamol pMDIs (Airomir® and Ventolin®) produced an aerosol with a mass median aerodynamic diameter (MMAD) that increased from approximately 2.0 to 3.7μm, when the testing environment was

changed from dry (37°C, <10%RH) to humid (37°C, >98%RH). The authors proposed three mechanisms in the transition from propellant spray to aerosol:

- The evaporating propellant leaves the remaining non-volatile particles cooled to a low temperature;

- The particles act as condensation nuclei for water vapour. As such, particles would be expected to grow larger in humid air, and increase in temperature due to heat flow from the surrounding gas phase;

- The final stage is water evaporation to reach equilibrium with the surrounding gas phase [59].

The aforementioned studies on pMDI aerosol behavior in hot and humid conditions employed mechanical ventilation setups to model the inhalational profile of intubated patients, and did not pay particular attention to mouth-throat deposition. The pMDI formulations tested were also exclusively salbutamol sulfate-in-propellant suspensions. To explore beyond the above existing studies, we made use of the Alberta Idealized Throat, an idealized replica developed from MRI and CT scans of human subjects, that has been demonstrated to be an *in vitro* mouth-throat deposition model in good agreement with other *in vitro* and *in vivo* aerosol studies [60-62]. In the present study, *in vitro* mouth-throat and lung deposition experiments are conducted with the Alberta Idealized Throat set in a controlled environment, to evaluate the effect of temperature and humidity on the deposition patterns of solution and suspension pMDI formulations.

2.2 MATERIALS AND METHODS

2.2.1 Materials

The three formulations selected for study were:

- BDP, with 13% w/w ethanol and 1.3% w/w glycerol, in HFA134a ('BDP HFA134a');

- BDP with 13% w/w ethanol in HFA227 ('BDP HFA227'); and

- Fluticasone propionate in HFA134a ('Flixotide Evohaler').

The differences in the composition and type of these formulations may be the basis for differences in droplet atomization and evaporation; and subsequently, expected to affect mouth-throat and lung deposition, in response to variation in temperature, relative humidity, and air flow rate.

The two experimental solution pMDI formulations, BDP HFA134a and BDP HFA227, were prepared at laboratory scale, both designed to contain 100µg beclomethasone dipropionate (BDP) per 50µL metered dose. All materials were of pharmacopoeial or approved pharmaceutical grade. Drug concentrates of BDP in ethanol or ethanol/glycerol were prepared by weight, then weighed into 19mL capacity aluminum canisters (C128; Presspart Manufacturing Ltd, Blackburn, Lancashire, UK), crimped with 50µL valves (BK357; Bespak Europe Ltd, Kings Lynn, Norfolk, UK), and finally filled to weight through the valve with propellant. These MDI units were then fitted

with actuators with a 0.30mm exit orifice (BK634, Bespak Europe Ltd, Kings Lynn, Norfolk, UK).

Flixotide™ (fluticasone propionate 250µg per dose) Evohaler™ suspension MDIs (Allen & Hanburys, Uxbridge, Middlesex, UK), and analytical grade methanol (Fisher Scientific, Ottawa, Ontario, Canada), were used as received.

2.2.2 Apparatus setup

A schematic of the experimental apparatus used in this study is shown in Figure 2-1. The Alberta Idealized Throat was coupled to a collection filter with a pore size of 0.3µm (Respirgard TM II 303; Vital Signs Devices, Totowa, NJ, USA). The air flow rate through the setup was generated by a vacuum pump (Kinney, Canton, MA, USA) and was measured by a Model 4043 digital mass flow meter (TSI Instruments, St. Paul, MN, USA), accurate to 2% of the reading.

To control temperature and relative humidity, the idealized throat and filter were positioned inside a modified environmental chamber with glove ports (CEO-910W-4; Lunair Environmental, Williamsport, PA, USA), and a compressed dry air (CDA; < 1% RH) line was connected to the chamber. MDIs intended for testing were placed in the chamber, and allowed to equilibrate at the set temperature and relative humidity, prior to shaking and actuation using the gloves. The humidity and temperature of the chamber was monitored by a humidity and temperature meter (Humicap HM70, Vaisala, Finland). The specifications of this meter claim temperature measurements to be

accurate to 0.2°C at 20°C, and humidity measurements accurate to 1% of the reading, between 0-90% RH.
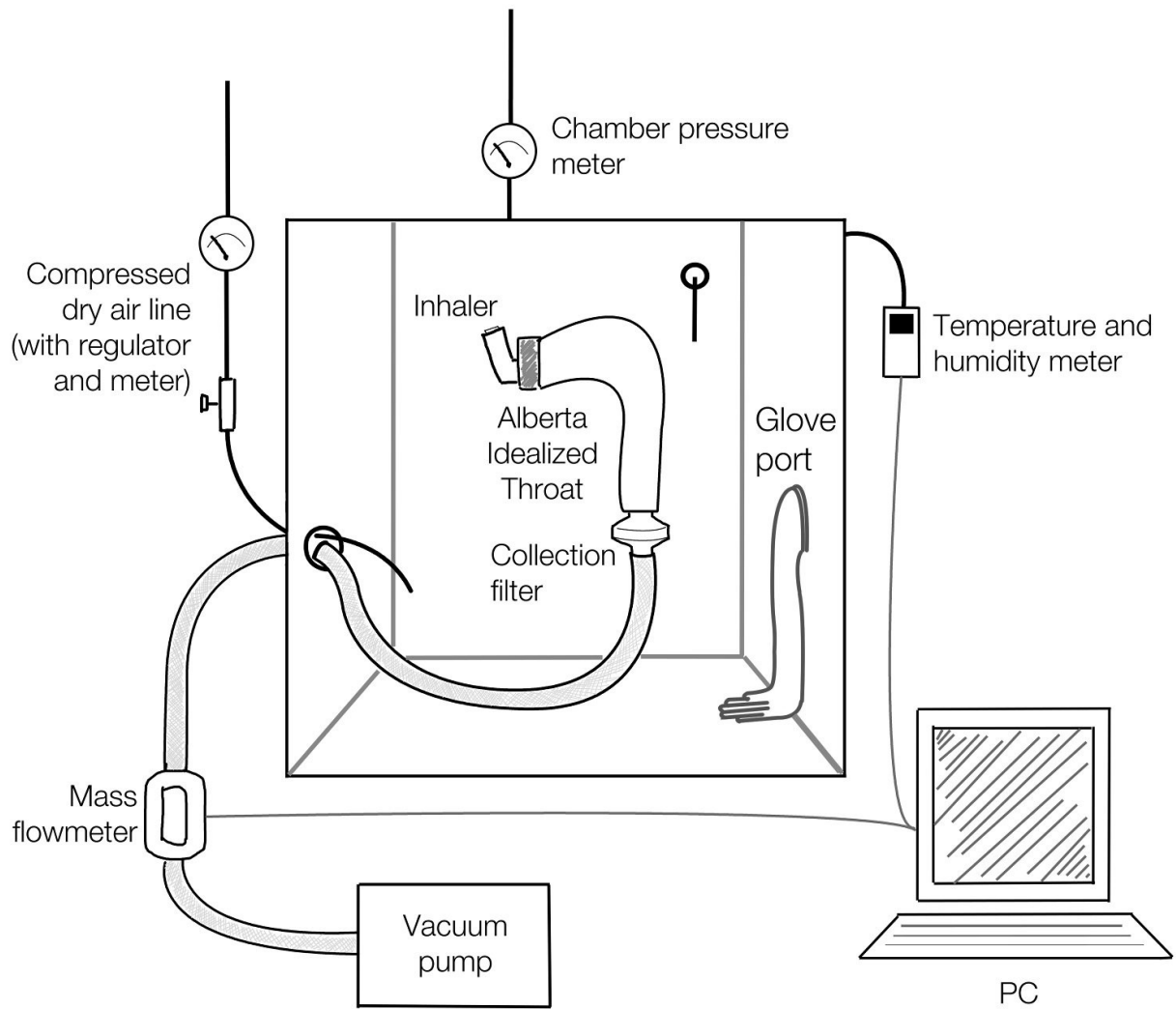
Figure 2-1 Schematic of the experimental setup.

2.2.3 Delivered dose uniformity

Each new pMDI (BDP HF134a, BDP 227, and Flixotide Evohaler) used in aerosol

dispersion testing was primed, by firing to waste five times at 1 min intervals. For

delivered dose uniformity testing, the apparatus setup in Figure 2-1 was modified – the

Alberta throat was removed, the pMDI mouthpiece was joined directly with an adaptor

to the inlet of a collection filter, and the filter outlet was connected to the vacuum pump.

Delivered dose uniformity was carried out at a single condition – 20°C, 35%RH,

28.3L/min. The pMDI was shaken for 5 sec, and a single shot was fired into the filter.

This was repeated four more times from a single pMDI. One pMDI was used for each

formulation.

The mass of the active pharmaceutical ingredient deposited in the filter was recovered

by rinsing twice with solvent (2 x 5 mL for BDP and 2 x 10 mL for Flixotide) and

quantified by UV spectrophotometry (2.2.5).
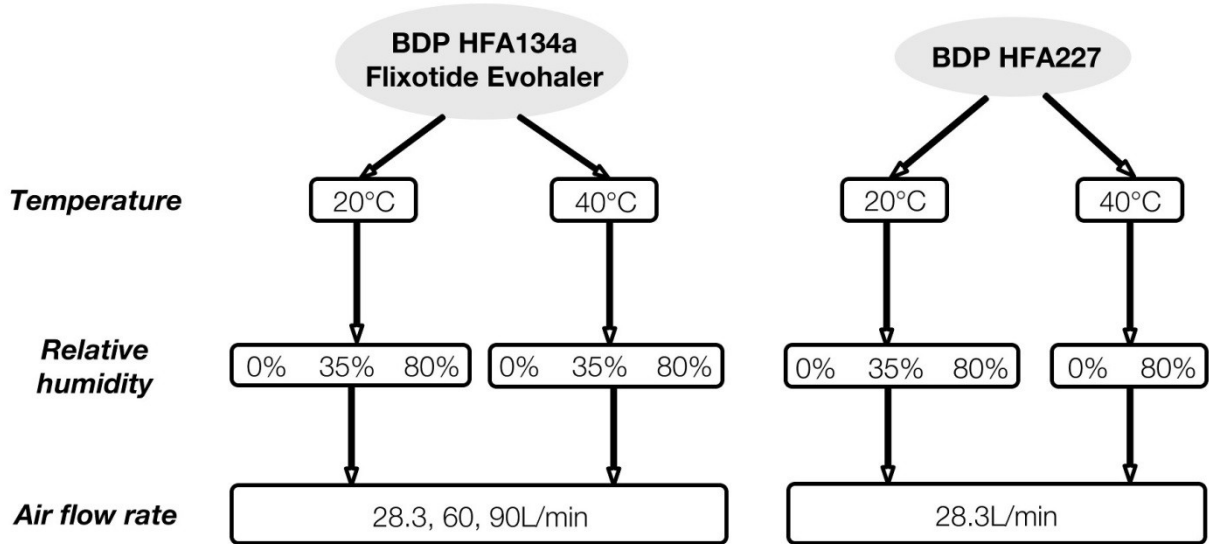
Figure 2-2 A diagram of the factorial design employed in this study to investigate the effect of experiment parameters temperature, relative humidity, and flow rate. Tests with BDP HFA227 only involved a single flow rate (28.3 L/min), and omitted 35% RH at 40°C.

2.2.4 In vitro aerosol deposition testing

The effect of three experimental variables were investigated – temperature (20 and 40°C), relative humidity (0 ± 1, 35 ± 2 and 80 ± 1 % RH), and flow rate (28.3, 60, and 90 L/min) – using the apparatus setup shown in Figure 2-1. However, while BDP HFA134a and Flixotide Evohaler were both tested at all three flow rates, BDP HFA227 was only tested at 28.3 L/min. A summary of the factorial design of this study is shown in Figure 2-2.

Before each test run, the Alberta idealized throat was sprayed with silicone oil (Molykote 316, Dow Corning Corporation, Midland, MI, USA) on the basis of work done by Zhou *et al.*, who demonstrated that the effect of particle bounce is minimized in

the Alberta throat, if it is grease-coated [62]. The pMDI canister was also weighed on an analytical balance (PI-225D, Denver Instruments, NY, USA) to give pre-actuation weight. The throat/filter assembly was placed in the chamber, along with the pMDI to be tested. The environmental chamber was closed, and the desired temperature and relative humidity was set. When the monitored conditions appeared to stabilize, the temperature and relative humidity was recorded for 5 min, at 1 sec intervals, to ensure that steady state was achieved, and the pMDI had been equilibrated to its surrounding conditions. The vacuum pump was also set to the desired flow rate during this period. The temperature, relative humidity, and flow rate reading was recorded before each test run.

Once recording was completed, the vacuum pump was switched on, the pMDI was shaken for 5 sec, connected to the throat inlet via an adaptor, and actuated. Afterwards, the pMDI canister was weighed to give the post-actuation weight. The throat and filter were rinsed, respectively, with 10mL and 5mL of methanol. The rinsate was collected in volumetric flasks and adjusted to volume with methanol. The pMDI actuator was wiped with a non-sterile cotton swab (Calapro, Yorba Linda, CA, USA) to collect actuator deposition. Experiments were conducted in triplicate (from a single canister) for each set of conditions in the experimental matrix.

2.2.5 Quantification and statistical analysis

The samples were assayed to quantify BDP and fluticasone deposition in the actuator, idealized throat, and filter. Chemical assays were performed by UV spectrophotometry (Model 8452A, Hewlett Packard, Greely, Ontario, Canada) at absorbance wavelengths of 238nm (BDP) and 236nm (fluticasone). Silicone oil did not produce absorption signals that would interfere with the assay.

The mass deposited in the filter was considered to be an in vitro measure of the amount of active pharmaceutical ingredient that reaches the lungs ('lung dose'). The 'recovered dose' was calculated as the sum of active pharmaceutical ingredient recovered from the pMDI actuator, idealized throat, and filter. The 'lung dose fraction' was defined as lung dose divided by recovered dose, expressed as a percentage. Drug deposition in the Alberta throat was also expressed as a percentage of recovered dose.

The percentage throat deposition and lung dose fraction results were subjected to one-way ANOVA analysis with Bonferroni post-test (GraphPad Prism 5.0, La Jolla, CA, USA), where a p-value < 0.05 was considered to be statistically significant.

2.3 RESULTS

2.3.1 Delivered dose uniformity

The delivered dose uniformity measurements, carried out at a single condition (20°C, 35%RH, 28.3L/min) gave results of 99.0 ± 6.1 µg for BDP HFA134a (n = 5), 99.0 ± 5.2 µg for BDP HFA227 (n = 5), and 256.0 ± 41.8 µg for Flixotide Evohaler (n = 5). Meanwhile, the average Flixotide shot weight across all flow rates and humidities was 73.6 ± 3.0 mg at 20°C, and 68.9 ± 5.2 mg at 40°C.
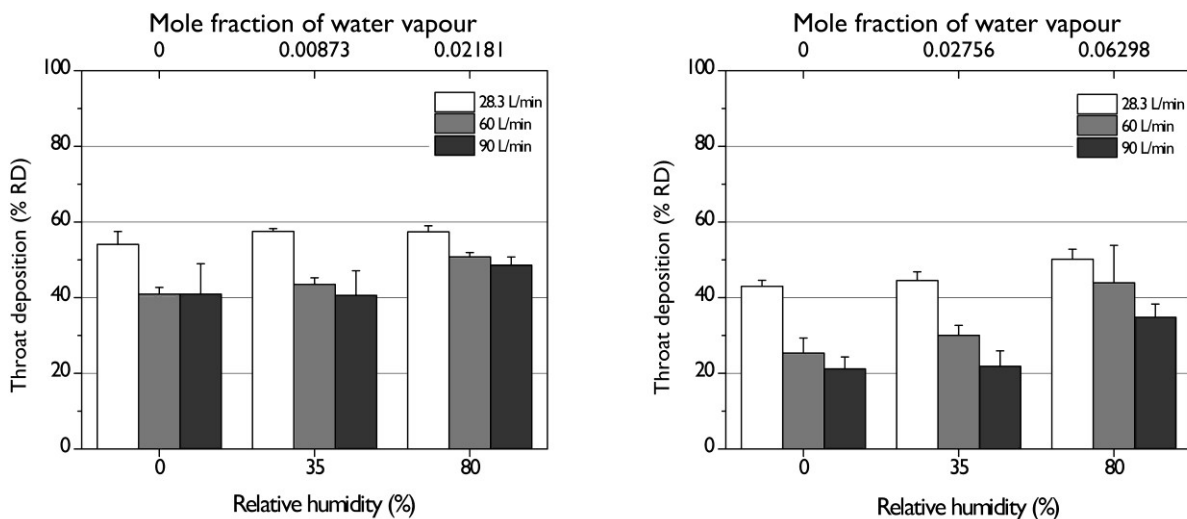
Figure 2-3 Mean percentage deposition of beclomethasone dipropionate (BDP HFA134a formulation) in the Alberta idealized throat (n = 3, mean ± S.D.), at 20 °C (left), and 40°C (right), at the three indicated flow rates (28.3, 60 and 90 L/min) and ambient humidities (0, 35 and 80% RH). Values given are % of recovered dose.
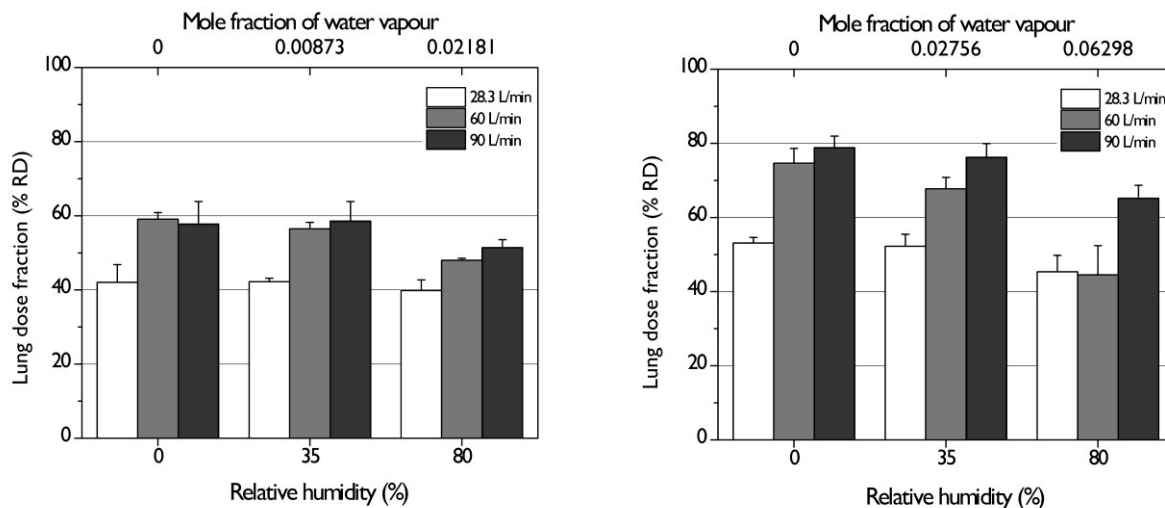
Figure 2-4 Mean lung dose fraction (n = 3, mean ± S.D.) of beclomethasone dipropionate (BDP HFA134a formulation) (n = 3, mean ± S.D.), at 20 °C (left), and 40°C (right), at the three indicated flow rates (28.3, 60 and 90 L/min) and ambient humidities (0, 35 and 80% RH). Values given are % of recovered dose.

2.3.2 Effect of relative humidity

For BDP HFA134a, the general observation is that there is little difference in throat deposition and lung dose fraction, between 0 and 35%RH conditions, irrespective of air flow rate or temperature (Figure 2-3 and Figure 2-4). The only exception to this is at 40°C and 60L/min, where the decrease in lung dose fraction (from 74.6 to 67.7%) was statistically significant ($p < 0.05$).

Between 35% and 80%RH conditions, there is a general increase in throat deposition, and decrease in lung dose fraction. This was statistically significant for all flow rates at 40°C, except for lung dose fraction at 28.3L/min (52.2 to 45.4%). At 20°C, the only

statistically significant results were at 60 L/min (43.5 to 50.8% in the throat, 56.5 to 48.0% lung dose fractions).

For BDP HFA227, there was no observable effect of relative humidity on throat deposition and lung dose fraction, at 20°C and 40°C (Figure 2-5). As shown in Figure 2-2, the 35%RH/40°C condition was not tested for this formulation.
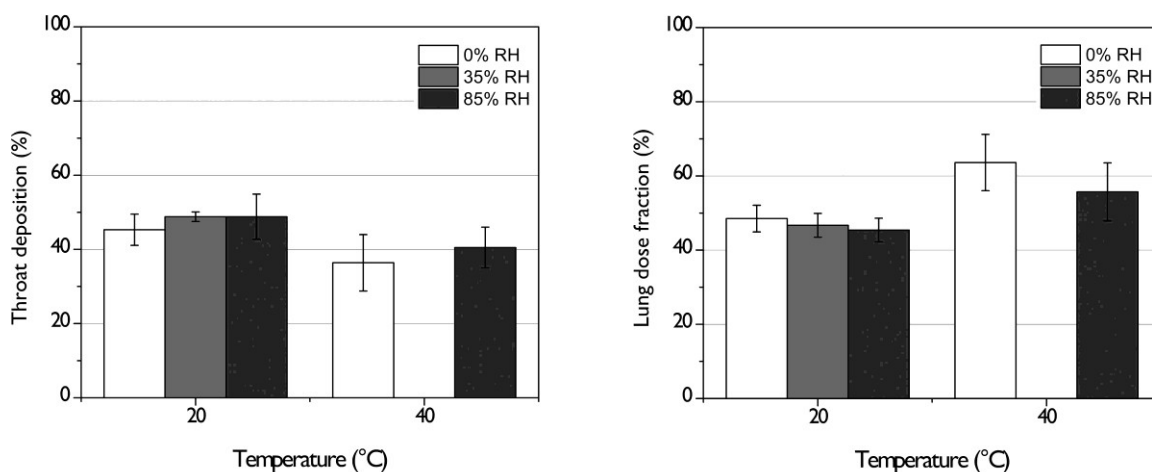
Figure 2-5 Mean percentage throat deposition (left) and lung dose fraction (right) of beclomethasone dipropionate for the BDP HFA227 formulation, at 28.3 L/min, the indicated relative humidities (0%, 35%, and 80%) and temperatures (20 and 40°C). Values given are % of recovered dose.

Fluticasone propionate deposition in the idealized throat increased with relative humidity irrespective of temperature or air flow rate (Figure 2-6). This general observation was statistically significant between 0 and 35% RH, and between 35% and 80% RH. The one exception is at 20°C and 28.3L/min, where the wider error bars for 35%RH result in only the difference in deposition between 0 and 80%RH being

statistically significant. Meanwhile, increasing relative humidity resulted in a

corresponding decline in lung dose fraction, statistically significant between 0 and

80%RH for all flow rates and temperatures.
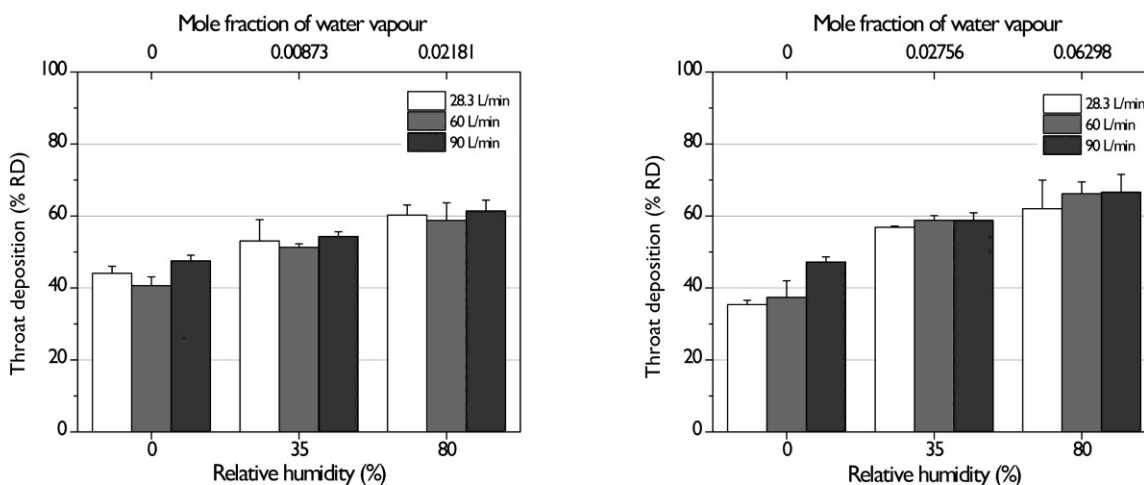
Figure 2-6 Mean percentage deposition of fluticasone propionate (Flixotide Evohaler) in the idealized throat ($n = 3$, mean ± S.D.) according to air flow rate (28.3, 60 and 90 L/min) and relative humidity (0, 35 and 80% RH) for 20°C (left) and 40°C (right). Values given are % of recovered dose.

2.3.3 Effect of temperature

Comparing between matching flow rate/relative humidity conditions at 20°C and 40°C,

the dominant observed trend for BDP HFA134a formulation was a lower deposition in

the throat, and greater lung dose fraction, at 40°C. This was statistically significant for

all flow rate/RH conditions, excepting the 60 L/min and 80%RH condition. For BDP

HFA227, decreased throat deposition and increased lung dose fraction was also

observed from 20°C to 40°C, but this was not statistically significant. There was

generally no significant difference in throat deposition and lung dose fraction for Flixotide Evohaler between 20°C and 40°C; the only exception was the 60L/min and 35% RH condition, where throat deposition increased (50 to 59%) and lung dose fraction decreased (45 to 39%).

2.3.4 Effect of air flow rate

Mean BDP deposition from the BDP HFA134a into the idealized throat and filter is shown in Figure 2-3 and Figure 2-4. For both temperatures it was observed that in throat deposition declined between flow rates of 28.3 to 60L/min ($p < 0.05$), with no further change at 90L/min. Lung dose fraction (Figure 2-4) increased from 28.3 to 60 L/min, at all relative humidities ($p < 0.05$), with no further change at 90 L/min. The only exception was the 40°C/80%RH condition, which showed a statistically significant decline in throat deposition and corresponding increase in lung dose fraction, when 28.3 and 90L/min results were compared.

At 35 and 80%RH, no significant effect of air flow rate was observed on mean fluticasone propionate (Flixotide Evohaler) throat deposition. At 0%RH, there is a statistically significant increase in throat deposition from 60 to 90L/min. Air flow rate did not appear to affect lung dose fraction, regardless of temperature or relative humidity ($p > 0.05$; Figure 2-6 and Figure 2-7, respectively).

The deposition results in Figure 2-3, Figure 2-4, Figure 2-6 and Figure 2-7were also plotted against the mole fraction of water vapour in air within each set of conditions. However, there were no clear trends observed for any of the formulations.
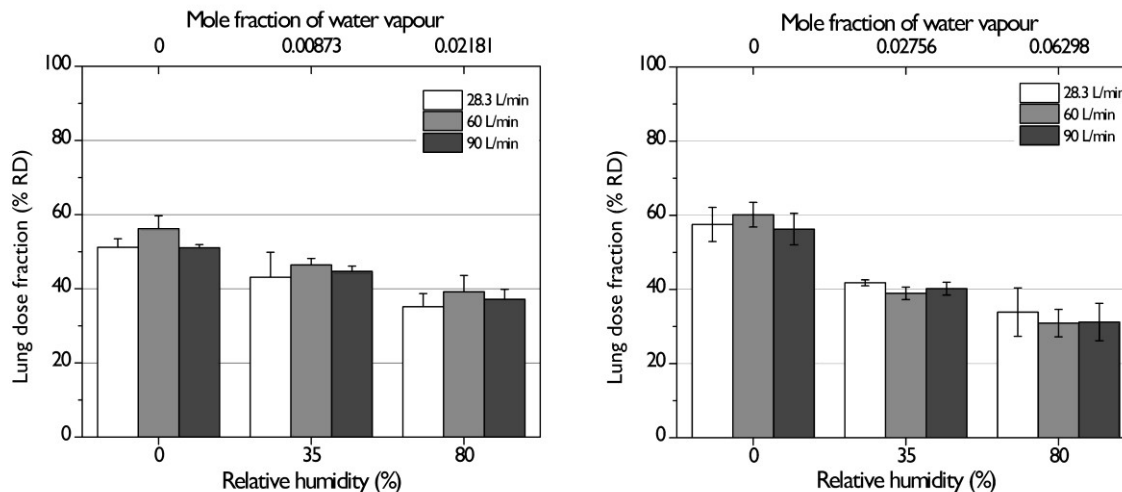
Figure 2-7 Mean lung dose fraction for fluticasone propionate (Flixotide Evohaler) ($n = 3$, mean ± S.D.) according to air flow rate (28.3, 60 and 90 L/min) and relative humidity (0, 35 and 80% RH) for 20°C (left) and 40°C (right). Values given are % of recovered dose.

2.4 DISCUSSION

The overarching message from the results in the current study is that the environmental conditions affect the *in vitro* delivery efficiency of solution (HFA134a and HFA227 MDI) and traditional suspension (Flixotide Evohaler) pMDI formulations. The extent of formulation response to the environment depends on the type of formulation, and the presence or lack of excipients. Relative humidity affects the suspension formulation more strongly than the solution formulations. Temperature affects the delivery of the

solution formulations, but had generally no effect on Flixotide. For both relative humidity and temperature variables, BDP HFA134a was more strongly affected than BDP HFA227.

Stein and Myrdal investigated the influence of ethanol concentration, on the theoretical droplet evaporation time for experimental pMDI formulations containing BDP and 1-20% w/w ethanol in HFA134a. Although ethanol has a higher wet bulb temperature (-1.3°C at 20°C, against -58°C for HFA134a), the much lower vapour pressure (6.32 kPa compared to 576 kPa for HFA134a at 20°C) was believed to be the deciding influence, reducing overall formulation vapour pressure, and increasing evaporation time [63]. Williams and Liu experimentally demonstrated a decrease in the vapour pressure of HFA134a and HFA 227 droplets at 25°C, with increasing ethanol concentration from 0 to 11.85% w/w [64]. The predicted consequence of increased evaporation time was larger droplets reaching and depositing in the mouth-throat, thus reducing lung delivery [63].

2.4.1 Relative Humidity

Brambilla *et al.* reported that the mean minimum plume temperature for Flixotide Evohaler was -51 ± 2.0°C at 20mm from the MDI mouthpiece, compared to -2.0 ± 1.9°C for a formulation similar to BDP HFA134a (50 µg BDP in HFA134a, with 12-15% w/w ethanol and 1.3% w/w non-volatile excipient) [65]. Flixotide's cold plume

37

temperature may be expected to enhance water condensation and could partly explain the effect of humidity with this formulation, as discussed further below.

A second factor which may also play a role in explaining our data relates to the number of particles present in the aerosol plume of the different formulations. Stein employed a mathematical model to estimate the number of HFA134a droplets collected in an Andersen Cascade Impactor from a single actuation. Flixotide Evohaler was estimated to produce 1 particle in 30 droplets collected; in comparison, the solution formulation QVAR® (BDP 100μg/dose, in HFA134a and ethanol co-solvent) is expected to yield one drug particle for every droplet actuated [20]. This may have implications for the post-actuation stage, where residual particles act as condensation nuclei.

The impact of relative humidity on particle deposition is likely to relate to condensation of water vapour on residual dry particles [59]. From this, we may reasonably expect that a higher relative humidity would result in a particle diameter increase, yielding greater mouth-throat deposition, and consequently a lower lung dose fraction. This was observed to greatest effect in the suspension formulation between 0 to 80% RH, giving 30% less lung dose at 20°C, and 40-50% less at 40°C. This may be explained by the rapid and complete evaporation of drug-containing and propellant-only droplets, leaving the relatively few and cold drug particles (see discussion of plume temperature and droplet number above) susceptible to condensation.

BDP HFA134a also demonstrated an increase in mouth-throat deposition and decrease in lung dose fraction with increased humidity, but in a weaker trend compared to

38

Flixotide. This could be due to both existing of less dried particles or potential nuclei in Flixotide plume as well as affecting droplet evaporation in BDP HFA134a and BDP HFA227 formulations by adding ethanol (and glycerol, for that matter).

The results may have implications for patients, who are commonly advised to store pMDIs below 25-30°C, according to label and patient information leaflets [66, 67]. From our results, in this condition (at 20°C), there is greater lung dose fraction in dry conditions (0%), and lower lung dose fraction in humid conditions (80%), showing that drug delivery could still be affected by environmental conditions, despite the storage advice given to patients.

2.4.2 Temperature

A factor to consider when interpreting the results is that the MDIs were placed in the environmental chamber before the temperature and relative humidity conditions were set. Consequently, the bulk formulation in the MDI was allowed to equilibrate with the chamber temperature before actuation of a dose. The vapour pressure of the bulk formulation is a function of the canister temperature and formulation composition. An increase in canister temperature from 20 to 40°C results in increased vapour pressure for HFA134a, HFA227 and ethanol in the bulk formulation, affecting atomization [63, 64].

Changes in atomization can affect lung delivery; however, while there was increased lung delivery at 40°C for BDP HFA134a (and to a lesser extent BDP HFA227), this was

not the case for the suspension formulation. Stein and Myrdal found formulation vapour pressure alone to be a weak predictor for fine particle delivery, compared to ethanol concentration and its effect on droplet evaporation time [63]. The differences in excipient content for the three tested formulations (solution MDIs contained 13% w/w ethanol, suspension MDI did not) appear to support this claim, as increased temperature did not affect lung delivery for all three formulations.

The observation of lower mouth-throat deposition at 40°C for BDP HFA134a (as well as for BDP HFA227, although not a statistically significant result) demonstrates decreased droplet evaporation time resulting in less droplet impaction in the mouth-throat. The dry particles pass through the throat, into the filter, leading to an increased lung dose fraction, which was seen in Figure 2-3, Figure 2-4 and Figure 2-5. However, the additional presence of glycerol in BDP HFA134a, with its low vapour pressure (0.0106 Pa at 25°C), did not appear to make a difference in lengthening droplet evaporation time, as lung delivery was not adversely affected in comparison with BDP HFA227.

As with flow rate, Flixotide Evohaler did not exhibit a significant change in deposition with temperature. This may be related to a short droplet evaporation time, due to the lack of ethanol and glycerol excipients that retard droplet evaporation.

2.4.3 Flow rate dependence

The existing literature for *in vitro* pMDI deposition has been largely based upon studies which are conducted in standard laboratory conditions (20-25°C, 35-45%RH). The trend at 20°C/35%RH in the current study, where mouth-throat deposition decreased from 28.3 L/min (58.9 ± 2.6 µg) to 60 L/min (45.3 ± 1.7 µg), with no further change at 90 L/min (40.5 ± 7.6 µg; Figure 2-2 and Figure 2-3), has been observed in a previous study by Rahmatalla *et al.*[37]. Also using the Alberta Idealised Throat and filter assembly, they investigated QVAR® pMDI (beclomethasone dipropionate 100µg/dose, in HFA134a and ethanol co-solvent) [64], which is a formulation similar to that used in the current study.

The flow rate dependence of mouth-throat deposition at low flow rates has been attributed to the differential between pMDI plume velocity, and inhalation flow velocity. The hypothesis is that a high velocity pMDI plume, upon encountering slower inhalational airflow, will result in a highly turbulent field that enhances deposition in the mouth-throat [37, 63]. However, the existing data on droplet velocities are variable, apparently depending on measurement technique, actuator orifice and valve design.

For instance, Dunbar *et al.* used phase-Doppler particle analysis (PDPA) to report an axial droplet velocity, for an HFA134a-only formulation, of around 50 m/s at 25mm distance from the actuator orifice [68]. Clark detailed another PDPA study of a CFC-12 formulation, which describes an axial droplet velocity of 35 m/s at 50mm from the orifice [69]. However, in a very recent laser Doppler anemometry (LDA) study by Liu

et al., Flixotide produced a mean droplet velocity of 16.3 ± 1.7 m/s at 30mm from the mouthpiece, while QVAR® produced 5.4 ± 0.1 m/s at the same distance [70].

The flow rates used in this study are equivalent to approximately 1 to 3 m/s through the mouth-throat. Based on the velocities measured by Liu *et al.* for QVAR®, the relatively small differential between plume and inhalational flow velocities suggests that changes in inhalation flow rate could cause major differences in the production of shear-induced turbulence, with higher shear at lower inhalation producing more turbulence. This may explain the higher mouth-throat deposition seen by us at 28.3 L/min for the present BDP HFA134a formulation.

Interestingly, the mouth-throat deposition results for the suspension-based pMDI, Flixotide Evohaler (Figure 2-6), do not exhibit this flow dependent behavior. This may be because the higher velocities measured by Liu *et al.* for this formulation yield shear-induced turbulence production that is unaffected by the small changes in differential velocities associated with changes in inhalational flow rate.

ACKNOWLEDGMENTS

AUTHOR DISCLOSURE STATEMENT
Authors David Lewis and Tanya Church are employees of Chiesi Ltd., Inc. No other conflicting financial interests exist.

Chapter 3.   An atomizer to generate monodisperse droplets from high vapor pressure liquids[1]

3.1 INTRODUCTION

The ability to produce monodisperse droplets and particles with sizes on the order of micrometers is important in many areas of experimental research related to the aerosol and pharmaceutical sciences [71]. Monodisperse aerosols have been used to study, for example, particle formation from evaporating solution droplets [72], the calibration of

---

[1] This chapter has been submitted to Journal of Atomization and Sprays as: Mehdi Azhdarzadeh, Farzin M. Shemirani, Conor A. Ruzycki, Alberto Baldelli, James Ivey, David Barona, Tanya Church, David Lewis, Jason S. Olfert, Warren H. Finlay, and Reinhard Vehring "An atomizer to generate monodisperse droplets from high vapor pressure liquids". Farzin M. Shemirani was responsible for designing, manufacturing and testing of the experimental setup and data analysis as well as assisting in writing the manuscript. Mehdi Azhdarzadeh assisted in design of the atomizer and the manuscript composition. Conor A. Ruzycki contributed in taking the tests. James Ivey assisted in discussing the data. Alberto Baldelli helped in setting up the test rig. David Barona assisted in manuscript writing as well as building the experimental setup. All the other authors shared the supervision of the project.

44

impactors [73], and the study of deposition in models of the human respiratory system [74]. A variety of methods including condensation-type aerosol generators [75, 76], vibrating orifice aerosol generators [42], fluidized beds [77], and spinning-top generators [78] can be used to generate micron-sized monodisperse aerosols. However, no currently available commercial product is capable of producing monodisperse droplets from high vapor pressure liquids such as HFA227ea and HFA134a, which are the most commonly used propellants in metered dose inhalers (MDIs) [79].

One method which has the potential for generating monodisperse droplets involves disintegrating a fluid jet by actuating a piezoelectric transducer [42]. This technique is based on the controlled disintegration of the jet column under the action of capillary waves produced by the piezoelectric transducer. For high vapor pressure liquids a potential problem is the flashing of the superheated liquid when exposed to atmospheric pressure, which interferes with the desired monodisperse disintegration of the jet. To overcome this issue, the flashing of propellant in the jet can be inhibited by increasing the liquid pressure, or decreasing the vapor pressure by cooling the propellant, or both.

In this project an atomizer based on controlled Plateau-Rayleigh jet breakup [42, 80] capable of producing micron-sized droplets was designed and prototyped to generate monodisperse droplets of high vapor pressure liquids. The geometric diameter range of 8-12 μm is the most common range for propellant droplets emitted from commercial MDIs [81]. To control propellant flashing, a high pressure feed system capable of

operating at pressures up to 2.7 MPa and a cooling circuit inside the atomizer capable of lowering the temperature of the propellant to $-30\ ^{\circ}\text{C}$ were incorporated.

3.2 THEORY AND METHODS

To design a new atomizer for high vapor pressure liquids it is essential to understand the theory behind jet disintegration. Rayleigh [82] studied the linear instability of an inviscid jet exposed to capillary waves, finding an approximation for the diameter of the resulting droplets through the assumption that jet breakup occurs by growth of the most unstable disturbance. Reviews of the theoretical analysis of jet instability have been conducted by Bogy [83] and Sirignano and Mehring [84].

According to Rayleigh [82] only waves with wavelengths larger than the circumference of the jet can grow. This finding can be expressed as a frequency limit for the external disturbance, f, as follows:

$$f < \frac{4\dot{V}}{\pi^2 d_j^{\ 3}} \tag{3-1}$$

Applied to a case where a liquid jet emerges from an orifice and the external disturbance is produced by a piezoceramic, f becomes the actuation frequency of the piezoceramic, $\dot{V}$ is the volumetric flow rate through the orifice, and d_j is the diameter of the jet. This equation does not provide a lower frequency limit for the actuation frequency.

For current commercially available vibrating orifice aerosol generators designers use an empirical equation to estimate the usable actuation frequency range. This equation was originally recommended for production of monodisperse droplets from vibrating capillary tubes [43]:

$$\frac{4\dot{V}}{7\pi d_j{}^3} \leq f \leq \frac{4\dot{V}}{3.5\pi d_j{}^3}$$

(3-2)

The initial geometric diameter of a droplet, d_d, for a given actuation frequency can be estimated by the volume of a jet segment with a length corresponding to the wavelength of the disturbance as follows,

$$d_d = \sqrt[3]{\frac{6\dot{V}}{\pi f}}$$

(3-3)

Assuming a jet diameter of d_j, Rayleigh [82] argued that the most unstable waves have a wavelength of

$$\lambda_{opt} = 4.508 \times d_j$$

(3-4)

Inserting equation (3-4) into equation (3-3), the geometric diameter of droplets for the most unstable waves is

$$d_d = 1.89 d_j$$

(3-5)

Using equation (3-3) along with the jet velocity, $v_j = C_d \sqrt{\frac{2\Delta p}{\rho}}$, and droplet center-to-

center spacing, $x = \frac{v_j}{f}$, the normalized droplet spacing is given by

$$\frac{x}{d_d} = \frac{v_j}{f d_d} = \left(\frac{4 C_d^2 \, \Delta \, p}{3\rho d_d^2 f^2}\right)^{1/3} \tag{3-6}$$

Figure 3-1, assuming an equal diameter for the jet and the orifice, presents the

recommended jet disintegration region for HFA227ea as a function of working pressure

and actuation frequency along with the expected droplet size, d_d, and normalized

droplet spacing, x/d_d. To stay in the common geometric diameter range for propellant

droplet emitted from commercial MDI's [81], an orifice size of 12 ± 1.9 μm is used in

the graph (Figure 3-1) and related experiment (Figure 3-4). The orifice diameter and its

uncertainty were reported based on scanning electron-microscopy (SEM) images of four

orifices used in the experiments. The upper and lower limits for the frequency were

chosen based on equation (3-2). The lower limit for the pressure range was chosen

based on the vapor pressure of HFA227ea at room temperature, i.e., 390 kPa at 20°C.
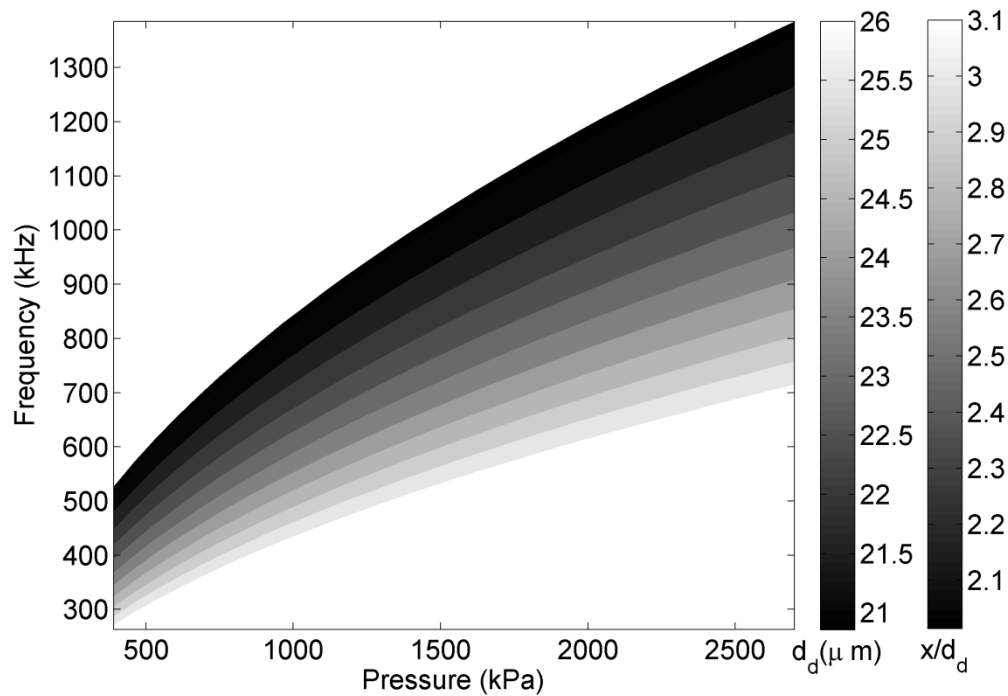
Figure 3-1 Recommended frequency range and expected droplet diameter d_d, (left hand column of legend) and droplet spacing $\frac{x}{d_d}$ normalized by droplet diameter (right hand column of legend) for different working pressures of HFA227ea, based on equations (3-2), (3-3) and (3-6), and an orifice diameter $D = 12 \pm 1.9$ μm.

In a similar fashion, a graph can be produced for HFA134a. The graphs will be only different due to density and vapor pressure differences that affect the emerging jet velocity and lower pressure limit respectively. It can be seen from the Figure 3-1 that as a consequence of the high working pressure required for handling of HFA227ea or HFA134a, actuation frequencies on the order of 10^5 to 10^6 Hz are required to achieve monodisperse atomization. This finding determines the required frequency response of the piezoceramic actuator used in the new atomizer design.

A schematic design of the atomizer with its main components labeled is depicted in Figure 3-2. Pressurized propellant is fed into the atomizer head (1) through the feed flow tubes (2). This pressurized liquid then fills up a reservoir between the orifice (9) and the atomizer head, while an O-ring (11) ensures a tight seal. Upon emerging from the orifice, a jet is formed from the pressurized propellant or propellant-solvent mixture. A disturbance is applied to the jet using a piezoelectric transducer (10) connected to a function generator through a spring probe (3). To prevent droplet coalescence, which may affect the degree of monodispersity, the chain of generated droplets is dispersed by a turbulent air stream provided by a dispersion air tube (13) in the orifice cup (8). Thermostatic tubes (6) and (7) build up a circuit of cooling fluid through the body of the atomizer (4) allowing for control of the propellant in the reservoir. According to Figure 3-1, the required actuation frequency for the production of propellant droplets in the 10 – 20 μm diameter range may exceed 1 MHz. At such a high frequency, the mechanical response of thin piezoceramics is more desirable and more efficient [85], so a thinner piezoceramic compared to commercial available counterparts, $t = 2$ mm, was utilized in the atomizer.
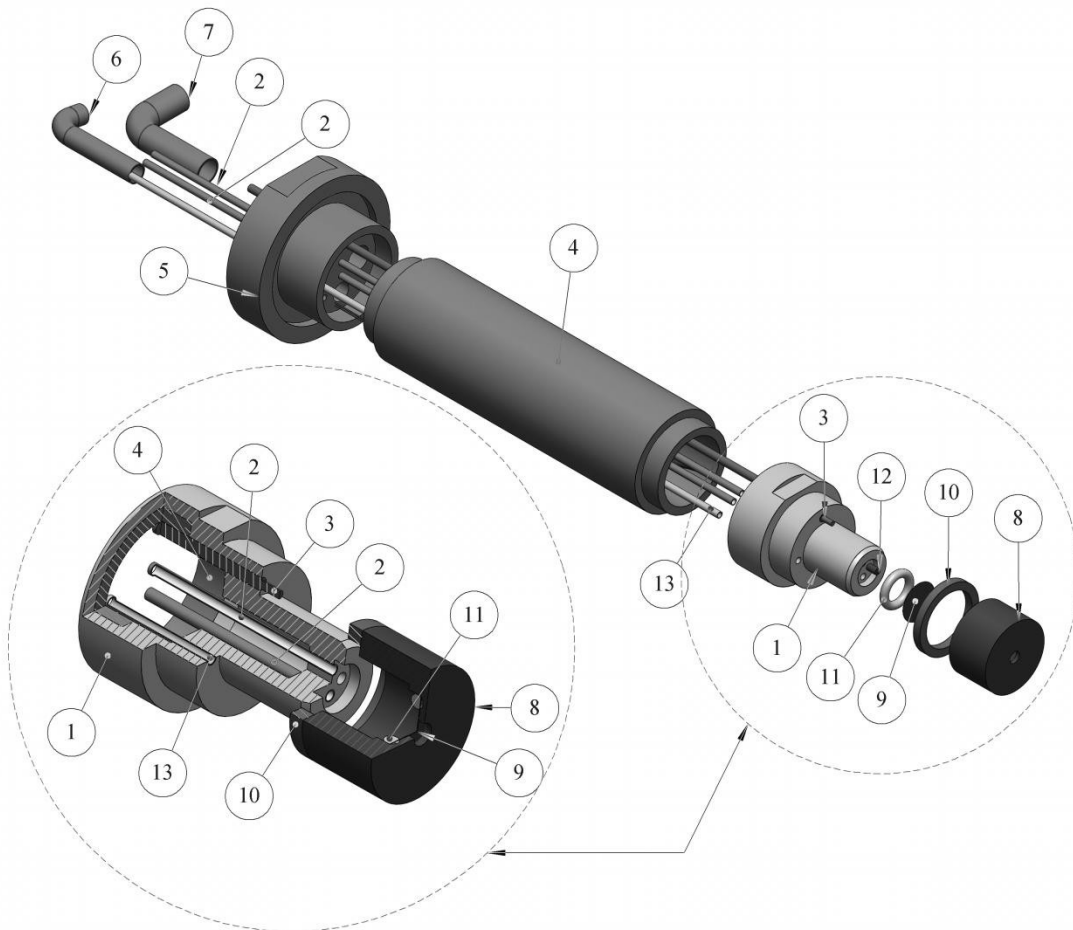
Figure 3-2 Schematic exploded view of the atomizer; 1. Atomizer head 2. Feed flow tubes, 3. Spring probe, 4. Atomizer body, 5. Atomizer base, 6.7, Feed tubes for thermostatic fluid, 8. Orifice cup, 9. Orifice plate, 10. Piezoceramic, 11. O-ring, 12. Thermocouple 13. Dispersion air tube

3.2.1 High pressure feed line and cooling circuit

A schematic of the propellant feed line along with the atomizer is depicted in Figure 3-3. To avoid internal flashing in the liquid feed, head space pressurization with nitrogen gas was implemented. The atomizer was also coupled to a cooling circuit to prevent external flashing of the jet upon emission from the orifice. A T-type

thermocouple (316-T-MO-062, Omega, Laval, Quebec, Canada) was inserted into the liquid bath before the orifice to monitor the liquid propellant temperature (Figure 3-2, (12)), allowing for the measurement of the cooled propellant temperature immediately prior to exiting the orifice. The working pressure of the system can be varied to a maximum of 2.7 MPa.
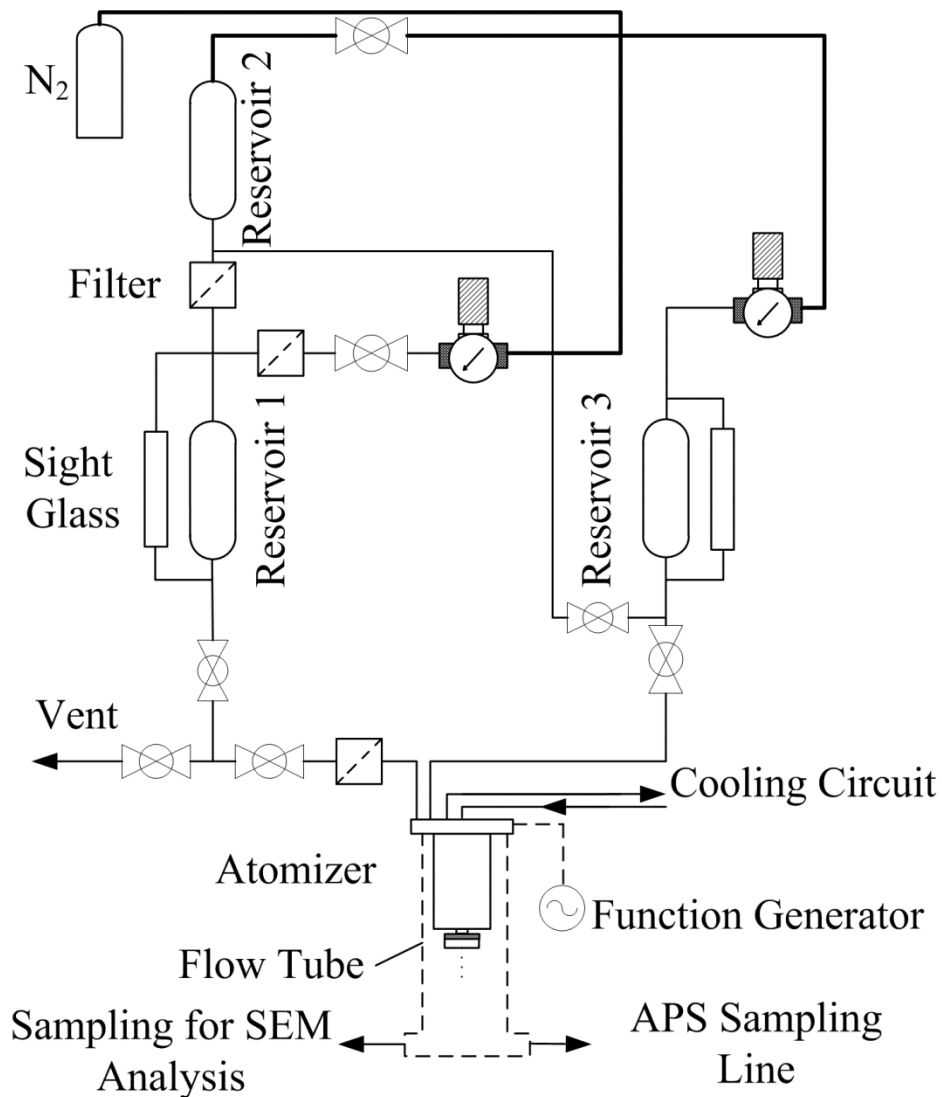
Figure 3-3 Schematic of the atomizer system with associated periphery.

Pharmaceutical grade HFA propellants, HFA134a and HFA227ea (Mexichem, Tlalnepantla, State of Mexico, Mexico), were fed into the system by first filling a portable reservoir (reservoir 2) with a propellant pump (Model 2008/100, Pamasol, Pfäffikon, Switzerland). The filled reservoir was then connected to the feed line, pressurized using high-pressure nitrogen, and filtered through a stainless steel frit-type filter with a pore size of 0.5 μm (SS-4TF-05, SS-4F-K4-05, Swagelok, USA).

After filling the system with the propellant, the system pressure was adjusted using a pressure regulator (Swagelok, KPR1JRF412A20000, USA). The third reservoir enables flushing of the system to clear any vapor bubbles from the feed system. As a final measure to avoid impurities from entering the atomizer, which could clog the orifice, two filters with 0.2 μm pore size (SS-4TF-05, , Swagelok, USA) were incorporated into the setup just before the atomizer. The use of the portable reservoir allowed filling the reservoir with formulations containing solutes in various HFA-type propellants prior to pressurization, providing a wide range of potential test fluids.

Cooling of the jet was achieved using heat transfer fluid (HC-C22A, Dynalene, PA, USA) circulated through the body of the atomizer using a circulating bath (A-40, Anova Inc., Stafford, TX, USA). The circulating bath allowed for cooling of the refrigerant liquid to -40 °C, which limited the minimal atomizer temperature to -30 °C.

3.2.2 Real-time measurement of droplet size, spacing, and velocity:

Droplet size was measured according to Fraunhofer forward scattering theory. For this purpose, a diode laser (DLSC 660 nm Coherent, Wilsonville, OR, USA) was operated at a wavelength of 657 nm and aligned to illuminate the liquid jet at a right angle. A screen located on the opposite side of the jet perpendicular to the laser beam captured the diffracted laser light pattern. Fraunhofer diffraction theory is only applicable to diffracted angles (measured relative to the laser light beam) less than approximately 10°. Theoretically, monodisperse droplets produce a pattern of concentric rings, where bright rings represent the angles of maximum intensity of the diffracted light. The relative position of these rings is a function of droplet diameter. By measuring the distance between the jet and the screen and radius of the rings, the diameter of droplets can be calculated [86]. As an example, the following relation can be used to determine the particle diameter, d_d, as a function of the angle of the second maximum of the scattering intensity,

$$d_d = \frac{1.64\lambda_l}{sin\,\theta_{2nd\,max}}$$
(3-7)

Here λ_l is the wavelength of incident light. Along with concentric rings, several horizontal lines were observed on the screen, caused by the evenly spaced droplets acting as a diffraction grating. The horizontal lines on the screen are the points of constructive interference for the diffraction grating phenomenon. The angle of these bright horizontal lines with respect to the laser light path, θ_m, is representative of the

droplet spacing, i.e., the distance between the center of successive droplets. The governing equation for this phenomenon is [87]:

$$x = \frac{m\lambda_l}{\sin\theta_m} \tag{3-8}$$

Here m is an integer representative of the order of the maximum used, x is the center-to-center droplet spacing, and θ_m is measured from the direction of the laser beam. After finding the droplet spacing, the calculation of the droplet velocity, v, is straightforward given knowledge of the frequency, f, applied to the atomizer, i.e., $v = xf$.

3.2.3 Dry Particle Generation and Collection

To test the capability of the setup in generating monodisperse solid particles, a solution containing 0.17% w/w beclomethasone dipropionate (BDP, 99.4% supplied by Chiesi Ltd, Chippenham, Wiltshire, UK), 13% w/w ethanol (USP grade anhydrous ethyl alcohol, Commercial Alcohols, Brampton, Ontario, Canada), and HFA134a was atomized into a confined flow tube using a piezoelectric transducer frequency of 450 kHz and amplitude of 10 V peak to peak as controlled by a function generator (Model DS340, 15 MHz Synthesized Function Generator, Stanford Research Systems, Sunnyvale, CA, USA). The confined flow tube acted as a drying column for atomized particles, with evaporation of propellant and ethanol resulting in dry particles. For this experiment the reservoir pressure was set to 1 MPa, and a 20 ± 3 µm orifice was fitted to the atomizer head. Compressed dry air was used to reduce the humidity within the

drying column, helping to avoid condensation and subsequent freezing of water on the orifice. A dedicated vacuum line was used to reduce the pressure inside the flow tube relative to ambient, providing a measure of safety against room contamination via aerosolized particles.

Dry particles were sampled from the drying column for electron microscopy as shown in Figure 3-3. Particles were collected using a modified Anderson Cascade Impactor (Anderson 1 ACFM Non-Viable Particle Sizing Sampler Mark II, Graseby Andersen, Smyrna, GA, USA). Only the collection plate downstream of the fifth stage was placed into the cascade impactor; all other stages were removed prior to testing to avoid sizing of the aerosol and ensuring that a representative size distribution could be collected and imaged with SEM. Several polycarbonate filters (ATTP01300 Isopore Membrane Filters, Millipore, MA, USA) were placed on the collection plate, allowing for sample collection on a suitable membrane for SEM imaging. Clear adhesive tape was used to close half of the total number of orifices on the fifth stage of the cascade impactor, concentrating the aerosol onto a smaller area of the downstream impaction plate while reducing the stage cutoff diameter from 1.1 μm to 0.65 μm at the standard flow rate of 28.3 L/min, produced by a vacuum pump (New Anderson Pump, Graseby Andersen, Smyrna, GA, USA). This concentration of aerosol allowed for shorter test durations and improved collection of particles in the respirable size range of 1 to 5 μm.

Using a second sampling line the monodispersity of the dry particles was monitored with a time-of-flight type particle sizer (APS 3321, TSI, Minneapolis, MN, USA) while

aerosol was drawn through the cascade impactor. After 10 minutes of sample collection, the feed line to the atomizer was closed, and the vacuum pump switched off. Filters were removed from the impaction plate and placed on aluminum sampling stubs, then gold coated (Desk II Gold Sputter Unit, Denton) and imaged using scanning electron microscopy (Model 1430 Scanning Electron Microscope, LEO).

3.3 RESULTS AND DISCUSSION

3.3.1 Monodisperse propellant droplets

Droplets of propellant HFA227ea were produced using a orifice with diameter of 20 ± 3 μm. The actuation voltage signal to the piezoelectric transducer was a square wave with 10 V (peak to peak) amplitude. The temperature of the jet was set to $-22°C$, and the liquid pressure was 1.2 Mpa. Droplet diameter and spacing were measured as described before by Fraunhofer diffraction. The stable diffraction patterns shown in Figure 3-4 display the features expected from a chain of regularly spaced monodisperse droplets, i.e., concentric rings and overlaid horizontal lines. This indicates that the atomizer indeed produced monodisperse, regularly spaced droplets.

It can be observed in Figure 3-4 that the distance between the horizontal lines decreases with increasing actuation frequency, which is expected as droplet spacing is inversely proportional to the actuation frequency, $x = \frac{v_j}{f}$.
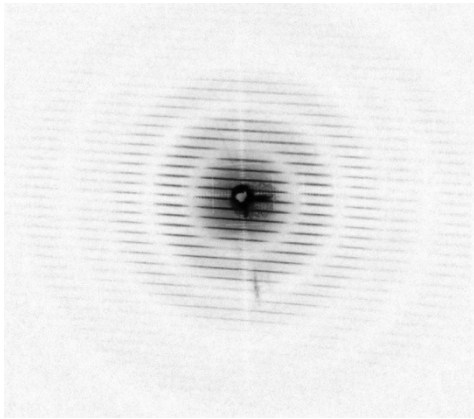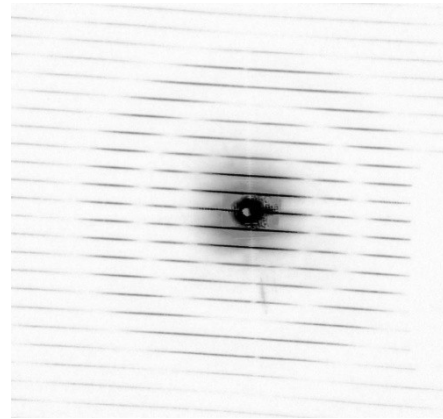
$$f = 290 \text{ kHz} \qquad\qquad f = 540 \text{ kHz}$$
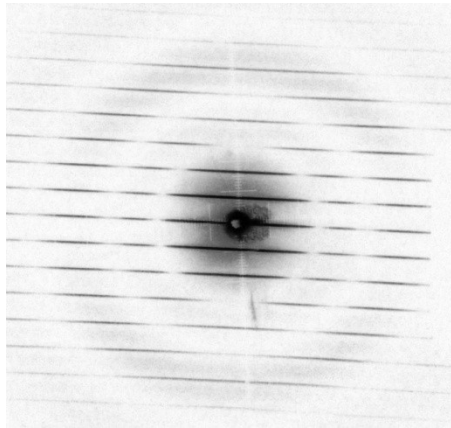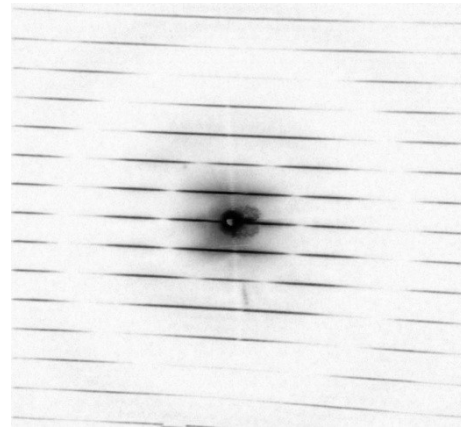
$$f = 750 \text{ kHz} \qquad\qquad f = 980 \text{ kHz}$$

Figure 3-4 Ring patterns and fringes (negative image) for HFA227ea confirming the monodispersity of droplets generated. Here the orifice diameter is $D = 12 \pm 1.9$ μm

Predicted droplet diameter, measured droplet diameter and spacing along with the uncertainty in their measurements are summarized in Table 3-1. Uncertainties were calculated using the equations for droplet diameter and spacing (equations (3-7) and (3-8)), assuming a maximum uncertainty of 1 mm in measurements for the location of

the rings, gratings and distance of the jet from the screen. The results are calculated

based on the scattering patterns in Figure 3-4. The initial jet velocity is calculated by

Bernoulli's equation assuming a discharge coefficient of 1.0 and predicted diameters

were reported using equation (3-3) and aforementioned discharge coefficient.

By comparing Figure 3-1 and Figure 3-4 it is observed that the low frequency case (290

kHz) and the high frequency case (980 kHz) are outside of the expected empirical

frequency range proposed by Schneider & Hendricks (1964). This contradiction

between Schneider & Hendricks' empirical result and the current result may be due to

differences in experimental conditions; unlike the high-pressure atomizer developed

here, Schneider and Hendricks [43]used a capillary tube to produce water droplets at 4.5

kHz. The current jet disintegration regime is also slightly different from the condition

used by Rayleigh to develop his theory of jet disintegration, specifically the assumption

of zero relative air velocity. It has been observed before that a high relative velocity

between the disintegrating jet and the surrounding air can decrease both the minimum

and optimum wavelengths for jet breakup [39]. Rayleigh proposed that the optimum

wavelength for jet breakup in air with zero relative velocity is 4.51 d_j, while Weber

showed that the optimum wavelength for jet breakup can be reduced to 1.3 d_j for a jet

with 35 m/s velocity. In Weber's case, air velocity amplified waves applied on the jet,

increasing the optimum frequency by over 300% to a value on the order of the

maximum frequency [39].

Table 3-1 Size, velocity and spacing for HFA227ea droplets measured by Fraunhofer diffraction theory and data from Figure 3-4.

Image	(a)	(b)	(c)	(d)
Frequency (kHz)	290	540	750	980
Predicted monodisperse droplet diameter (μm)	31	25	22	20
Measured monodisperse droplet diameter (μm)	35 ± 1.4	28 ± 0.9	25 ± 0.7	19 ± 0.4
Predicted droplet spacing (μm)	141	76	55	42
Measured droplet spacing (μm)	173 ± 11.6	86 ± 2.8	66 ± 1.7	52 ± 1.0

3.3.2 Solid monodisperse particle generation

Dry particles were generated from a solution of 0.17% w/w beclomethasone dipropionate (BDP), 13% w/w ethanol, and HFA134a, using the setup as described previously. Figure 3-5 shows a representative electron micrograph of the dried BDP particles. The particles are extremely uniform in diameter and morphology, with a slightly rugose surface and a single dimple. The geometric standard deviation of the particles, as reported by the Aerodynamic Particle Sizer was less than 1.2. Figure 3-6 depicts the cumulative mass distribution of the aerodynamic diameter for the BDP particles. The monodisperse, monomorph particles demonstrate a high degree of control over the droplet formation and propellant evaporation process, further confirming that the present technique can be used to generate particles with uniform properties from materials dissolved in high vapor pressure liquids such as HFA134a.
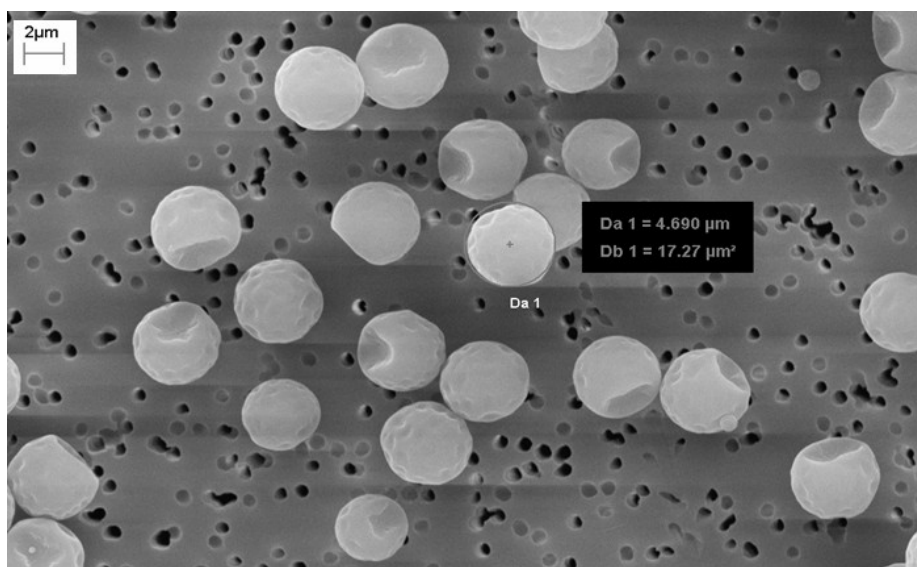
Figure 3-5 Scanning electron microscope picture of beclomethasone dipropionate particles atomized and dried from a solution of 0.17% w/w BDP, 13% w/w ethanol, and HFA134a showing monodispersity of the residual particles. A small number of satellite droplets are also visible in the image. Holes in the background are pores of the membrane filter used for capturing of the particles.
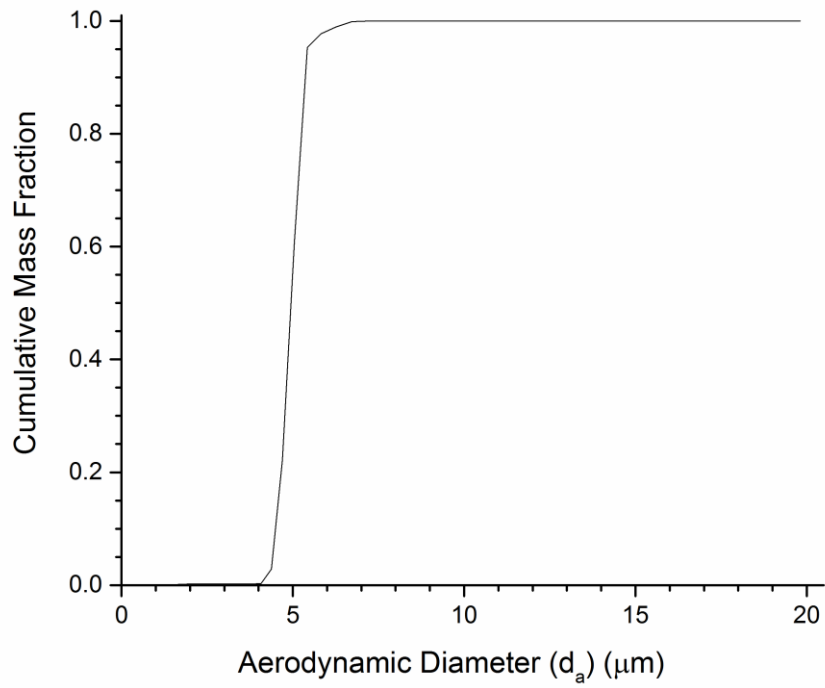
Figure 3-6 Cumulative mass fraction diagram for the BDP particles

Nomenclature:

C_d	Discharge coefficient of jet
d_j	Jet diameter
D	Orifice diameter
d_d	Droplet diameter
d_p	Particle diameter
f	Frequency
m	Diffraction order
p	Pressure
t	Thickness of piezoelectric transducer
$\dot{V}$	Volume flow rate
x	Droplet center to center spacing
v_j	Initial jet velocity
θ_m	Constructive interference angle
λ	Wavelength
ρ	Density

Chapter 4.   Onset of flash atomization in a propellant micro-jet[1]

4.1 INTRODUCTION

4.1.1 Pressurized metered dose inhalers

Pressurized Metered dose inhalers (pMDIs or MDIs) are the most common inhalation devices for pulmonary drug delivery. They are used in the treatment of asthma and chronic obstructive pulmonary disease (COPD), among other diseases. They produce a high speed spray plume containing millions of volatile droplets in a fraction of second, using liquids with high vapor pressures, e.g. HFA134a or HFA227ea, as propelling

---

[1] This chapter has been submitted to Journal of Fluids Engineering as: *Farzin M. Shemirani, Tanya K. Church, David A. Lewis, Warren H. Finlay, Reinhard Vehring as: "Onset of flash atomization in a propellant micro-jet"*. Farzin M. Shemirani was responsible for design of the experiment, running the tests, and composition of the manuscript. Tanya Church, David Lewis, Warren Finlay and Reinhard Vehring served as supervisors of the work.

agents [12, 18]. To solubilize the active pharmaceutical ingredients in the formulation containing propellants, ethanol is often used as a co-solvent. Because of the widespread use of these devices, the study of atomization processes involved in the production of the MDI spray has been the focus of several studies. Previous authors have proposed flash atomization or air-blast atomization [68, 69] as the dominant mechanisms involved in this spray production. The former mechanism is discussed here.

4.1.2 Flash atomization background

Flash atomization involves the rapid growth of bubble nuclei and the consecutive disintegration of the continuous liquid phase. The bubble nuclei can be formed either by homogenous or heterogeneous nucleation. Homogenous nucleation occurs within the liquid phase mostly at high degrees of superheat when the transient fluctuations in molecular density can create local densities close to that of saturated vapor [48]. On the other hand, heterogeneous nucleation occurs at already existing vapor bubbles when the liquid phase is in contact with another phase, which in MDIs would be the canister wall, suspended drug particles or impurities. Because heterogeneous nucleation requires a much lower degree of superheat to commence than for homogeneous nucleation [48], the former is much more likely to happen in flashing of pMDI sprays.

Flash atomization occurs in metastable flows, i.e. flows not having enough time for vapor bubbles to grow and reach thermal equilibrium. It is known that in practical applications, ejection of a high pressure liquid through an orifice plate into an

environment with pressures lower than the saturation pressure of the liquid produces a metastable flow [51]. This process is similar to what occurs in the metering valve of a pMDI (see section 4.1.3)

4.1.3 Flash atomization in MDIs

A schematic diagram of different components of a metered dose inhaler is shown in Figure 4-1. The formulation (1) is kept inside a container (2) which itself is located inside the actuator (6). The metering volume (3) holds a known amount of the mixture ready to be released to the ambient. By depressing the canister inside the actuator, the valve stem (5) slides through the metering valve and pressurized formulation then passes through the metering valve (4), valve stem and actuator orifice (7).
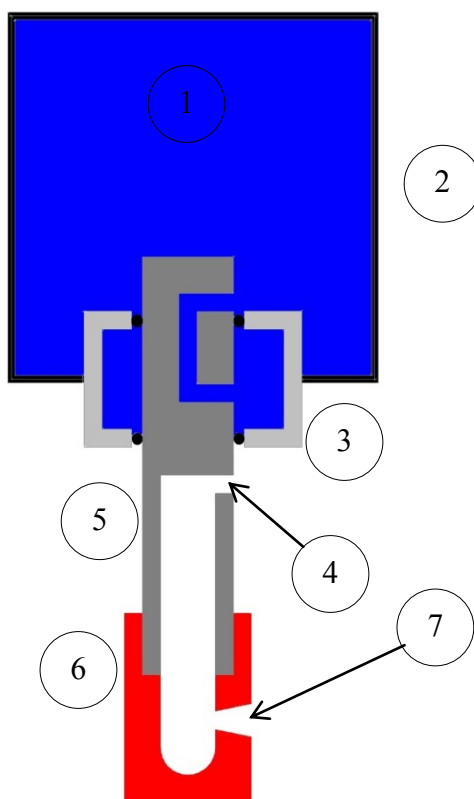
Figure 4-1 Schematic of different components of a metered dose inhaler: (1) formulation, (2) container, (3) metering volume, (4) metering valve, (5) valve stem, (6) actuator, (7) actuator orifice.

After depressurization, the liquid rapidly turns into a two-phase flashing flow to reach thermodynamic equilibrium at atmospheric pressure [6]. Several researchers have investigated the atomization process of MDIs. According to Dunbar [88] the atomization process in MDIs occurs in two different stages: primary atomization and secondary atomization. Primary atomization is the process of disintegration of the bulk liquid to individual droplets. Secondary atomization includes all the transport processes experienced by the droplets following the primary atomization. Dunbar [68] performed a flow visualization study on the near orifice flow of CFC and HFA134a containing

mixtures and suggested that the spray was pre-atomized in the actuator nozzle so that the primary atomization process was due to flash evaporation happening there. Clark [89], on the other hand, measured particle size distributions produced by MDIs using an aerodynamic particle size analyzer and proposed a correlation for the mass median aerodynamic diameter of the primary droplets. The similarity of this correlation to those describing air-blast atomizers led to the suggestion that aerodynamic breakup is the primary atomization mechanism.

Finlay [27] lists flashing or cavitation as major source of atomization in MDIs due to existence of numerous cavities and trapped vapor bubbles on the walls of the metering valve and actuator nozzle. Versteeg et al. [31] conducted a visualization study on flow pattern and spray of metered dose inhalers. They found that the flow in the expansion chamber is dominated by strong flash evaporation of the propellant and they observed the existence of an annular flow with vapor core in the both expansion chamber and spray orifice. They concluded that flash evaporation is responsible for the existence of very fine droplets in the spray, whereas, larger droplets are produced in the final stages of atomization because of the cessation of flashing at low liquid temperatures. This implies that evaporative cooling of the liquid propellant can impede flash atomization.

4.1.4 Flash atomization of droplets

Vapor bubble growth in flash evaporation of superheated liquid droplets has been studied both experimentally and theoretically. Experimental studies have been mostly

done on droplets suspended in a host liquid phase so that the evaporation at the droplet outer surface is avoided [90, 91]. Theoretical study of the vapor bubble growth within a single droplet is complicated because it demands the inclusion of stability analysis of the bubble surface in order to estimate the bubble growth rate [92, 93]. The theory of evaporation at the outer surface of a superheated droplet was described in detail by Kolev [94].

Razzaghi [95] proposed the idea of successive droplet breakups due to growth of the single bubbles available inside each droplet. Droplets break up to the point where the inside temperature is no longer sufficient for internal boiling. This finding clearly shows that flash atomization or bursting of droplets can be controlled by controlling the droplet temperature.

4.1.5 Flash atomization of jets and dimensionless numbers

Kitamura et al. [96] investigated the effect of the degree of superheat on the onset of flashing for water and ethanol jets having diameters between 0.36-1.6 mm. They described the onset of flash atomization in terms of dimensionless groups, Jakob and Weber numbers as follows:

$$Ja\,\phi = 100We^{-\frac{1}{7}}$$

(4-1)

$$Ja = \frac{\rho_L c_{pL}(T - T_{sat})}{\rho_g \Delta H_v} \qquad (4\text{-}2)$$

$$We = \frac{\rho_g d_j v_j^2}{\sigma} \qquad (4\text{-}3)$$

$$\phi = 1 - exp\left(2300 \frac{\rho_g}{\rho_L}\right) \qquad (4\text{-}4)$$

Here, Ja is the Jakob number, ϕ is the correction factor, We is the Weber number, ρ_L is the liquid density, c_{pL} is the specific heat capacity of the liquid at constant pressure, T is liquid temperature prior to leaving the nozzle, T_{sat} is the saturation temperature corresponding to the nozzle pressure, ρ_g is the vapor density, ΔH_v is the enthalpy of evaporation, d_j is the jet diameter, v_j is the jet velocity, and σ is the liquid-vapor surface tension. Equation (4-1) implies that as the jet velocity increases the amount of superheat required for the flash atomization decreases. The Jakob number is the ratio of sensible heat available for bubble growth to the latent heat of evaporation acquired by the vapor bubble. The use of the Jakob number in equation (4-1) was justified by the presence of a Jakob number term in analytical solution for the bubble growth rate [96, 97]. The Weber number is the ratio of inertial forces on the surface to the surface tension force. The use of the Weber number in equations concerning jet disintegration originates from findings of Weber who observed different cylindrical jet breakup patterns at different Weber numbers; namely, Rayleigh breakup and sinuous breakup regions [97].

4.1.6 Post-nozzle flashing

Flashing in jets exiting a nozzle can happen either insider or outside of the nozzle. Reitz [98] conducted a photographic study of flash atomization in a superheated water jet with diameter of 0.34 mm and attributed the jet disintegration to growth of bubbles outside the nozzle, *i.e.*, external flashing. This implies that the temperature of the jet even after the nozzle was high enough to cause flash atomization. In the case of HFA134a droplets, post-nozzle flashing was observed by Zhifu et al. [99]. They measured droplet velocities of an HFA134a flashing spray exiting a nozzle with a diameter of 0.81 mm. They observed an increase in the droplets' axial velocities downstream of the nozzle exit. This acceleration was explained by explosive flashing of the spray downstream of the nozzle. The same velocity increase was also observed at the same axial distance in the radial velocity profile. This finding implies that flash atomization of droplets could continue in droplets to the point where it stops due to evaporative cooling.

4.1.7 Heat and mass transfer in a superheated droplet

The heat and mass transfer processes involved in an isolated droplet are shown schematically in Figure 4-2. Here, for descriptive purposes only, processes are illustrated for a single droplet instead of a jet. If a bubble exists within a superheated liquid droplet having an initial temperature of T_0 higher than the boiling point of the droplet, T_b, at ambient pressure, p_{amb}; i.e. $T_0 > T_b\{p_{amb}\}$, the bubble starts to grow

because of the high saturation pressure present in the bubble, which is higher than the liquid or ambient pressure according to the Rayleigh-Plesset equation [100]. The determining factor for the vapor bubble pressure is the temperature at the liquid-bubble interface. As evaporation progresses, the droplet bulk temperature decreases through both internal and external evaporative cooling, assuming that the evaporation process is so fast that all the heat required for evaporation is provided by the liquid phase not the gas phase. If evaporative cooling is rapid enough, it can reduce the liquid phase temperature as well as liquid-bubble interface temperature to its boiling point at ambient pressure and impede the bubble growth by lowering the pressure within the bubble. Evaporative cooling of the droplets stops when reaching the wet bulb temperature, T_{wb}, which is well below the boiling point.

4.1.8 Current study

The current study investigates the effect of length scale, temperature, and formulation on the onset of flash atomization to determine if there exists a length scale at which flash atomization is inhibited by cooling. Due to the microsecond time scales involved in the evaporative cooling rate and bubble growth rate in superheated propellant droplets [92], individual droplets for experimental studies are exceptionally difficult to produce and study. Therefore, a steady jet of propellant emerging from a micro-orifice is produced, to investigate the onset of flash atomization.
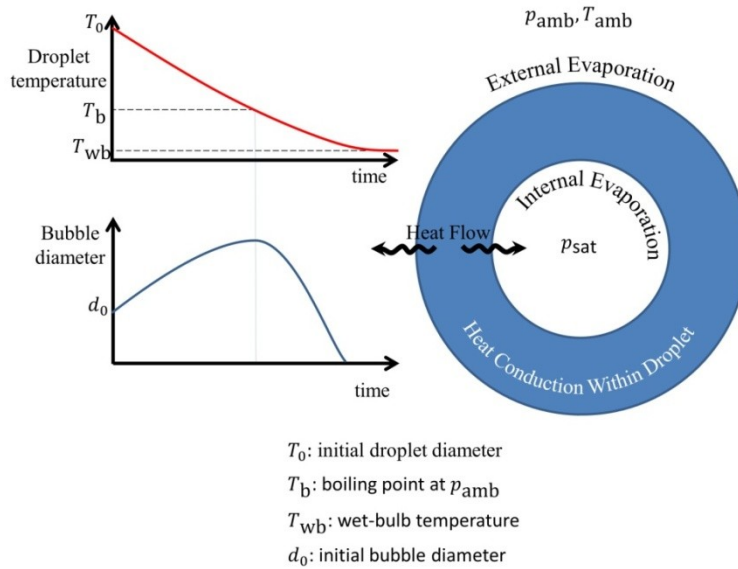
Figure 4-2 Schematic of heat and mass transfer processes involved in an isolated droplet with a bubble located at its center

4.2 EXPERIMENTAL SETUP

An atomizer was designed and manufactured to produce jets of mixtures of propellant and ethanol. Figure 4-3(a) shows an exploded view of the atomizer.

(a)   **(b)**
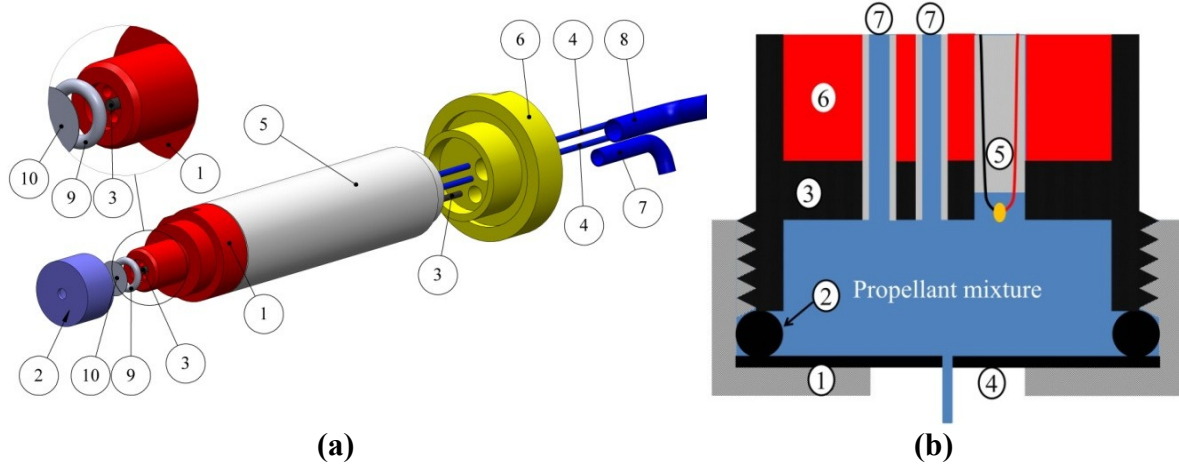
Figure 4-3**(a)** The atomizer used in the current study: (1) nozzle head, (2) orifice cup, (3) T-type thermocouple, (4) tubes for feed solution, (5) atomizer body, (6) base, (7) thermostatic liquid inlet tubing, (8) thermostatic liquid outlet tubing, (9) EPDM O-ring, (10) micro-orifice plate **(b)** Schematic of the feed reservoir: (1) orifice cup, (2) EPDM O-ring, (3) nozzle head, (4) micro-orifice plate, (5) T-type thermocouple, (6) thermostatic liquid, (7) tubes to feed the reservoir

This atomizer was equipped with two 1/16" tubes to feed the working fluid and drain it if needed. Two tubes were coupled to the base of the atomizer to circulate a thermostatic fluid (HC-C22A, Dynalene, PA, USA) to adjust the temperature of the feed flowing in a shell and tube type heat exchanger design surrounded by head, body and base of the atomizer, as shown in Figure 4-3(a). The thermostatic fluid temperature itself could be adjusted using a refrigeration bath (A-40, Anova Inc., Stafford, TX, USA). After passing through the head, pressurized liquid feed entered a small bath (Figure 4-3(b)) formed between the head, EPDM O-ring, and the orifice plate (Precision pinholes, Edmund Optics Inc., Barrington, NJ, USA). Dimensional tolerances and thicknesses of all the orifice plates used are shown in Table 4-1.

74

Table 4-1 Dimensional tolerances and thicknesses of the orifice plates used according to the manufacturer [101]

Orifice diameter (µm)	Dimensional tolerance (µm)	Thickness (µm)
5, 10	±1	12.7
15, 20, 25	±5	12.7
30, 35	±5	25.4

The EPDM O-ring was selected because of chemical compatibility with both ethanol and HFA propellants. The temperature of the small reservoir which feeds the jet, called the initial temperature, was monitored using a T-type thermocouple (316-T-MO-062, Omega, Laval, Quebec, Canada). All the parts used in the atomizer except the O-ring and orifice plate were made of 316-stainless steel. The atomizer could be operated at pressures up to 27 bars for hours. High pressurization of the atomizer head space was necessary to keep the highly volatile propellant mixtures in the liquid phase. The saturated vapor pressures (absolute pressure) of HFA134a and HFA227ea at 20°C are 572 and 390 kPa respectively.

A schematic diagram of the feed system used in the current study is depicted in Figure 4-4. To add the desired mixture to the system, first the portable reservoir was filled with a known amount of ethanol (USP grade anhydrous ethyl alcohol, Commercial Alcohols, Brampton, Ontario, Canada). Then, HFA134a (DuPont, Mississauga, ON, CA) or

HFA227ea (Mexichem, Tlalnepantla, State of Mexico, Mexico) was added to the reservoir using a diaphragm type propellant pump (Model 2008/100, Pamasol, Pfäffikon, Switzerland). To assure the accuracy of the ethanol concentration the portable reservoir was weighed before and after each filling with ethanol or propellant using a balance (XS4002S, Columbus, OH, USA). Then, the mixture in the portable reservoir was transferred to the main reservoir of the feed system using quick connect fittings coupled to the reservoir. Pressurization of the highly volatile mixture was achieved using a pressurized nitrogen tank and the pressure was adjusted using a pressure regulator (Swagelok, KPR1JRF412A20000, USA). Head space pressure (gauge pressure) was always kept at 1.2 MPa. In the feed system the liquid mixture and the nitrogen were filtered using filters with a pore size of 0.5 μm (SS-4TF-05, SS-4F-K4-05, Swagelok, USA) to prevent clogging of the micro-orifices. As depicted in Figure 4-4, the atomizer itself was placed in a sealed flow tube to allow adjustment of the ambient conditions. All the mixture combinations tested in the present study are tabulated in Table 4-2.

Table 4-2 Experimental data matrix

Ethanol concentration, w/w (%)	HFA134a Orifice diameter (μm)	HFA227ea Orifice diameter (μm)
0	5, 10, 15, 20, 25	5, 10, 15, 20, 25
10	5, 10, 15, 20, 25	5, 10, 15, 20, 25
15	N.A.	15, 20, 25, 30
20	5, 10, 15, 20, 25	20, 25, 30, 35
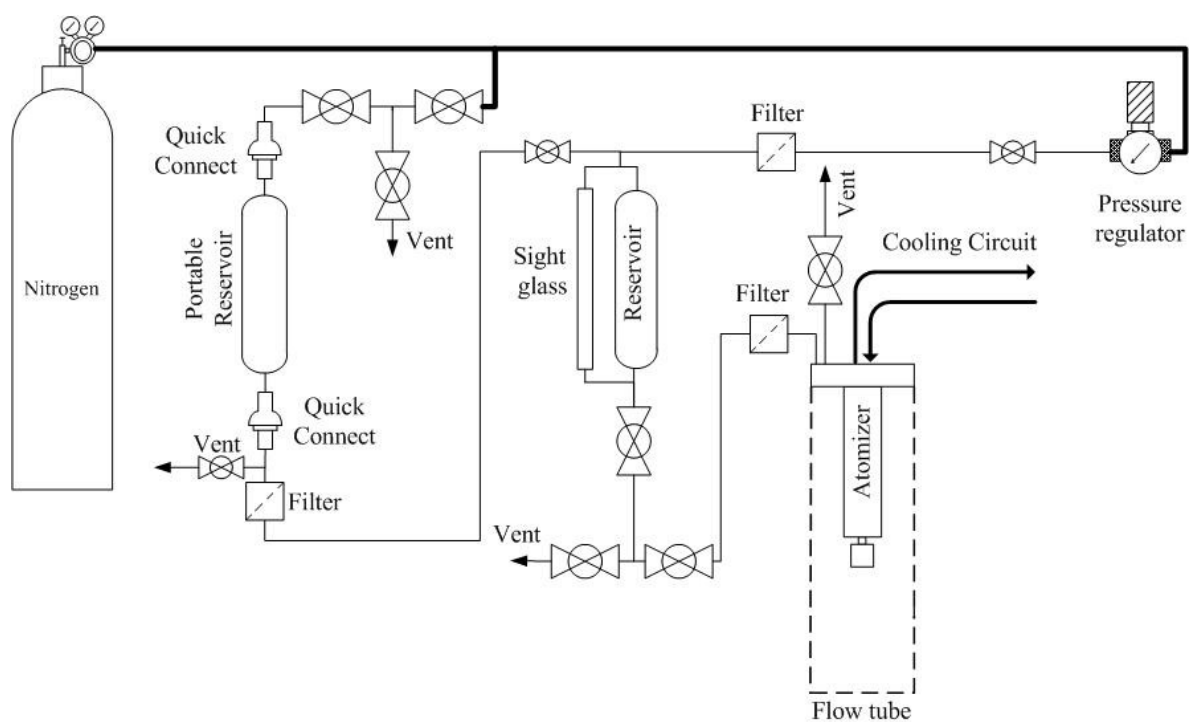
Figure 4-4 Schematic diagram of the experimental setup

Dry air was supplied to the flow tube at a flow rate of 20 L/min, resulting in a velocity

of 0.042 m/s around the jet. To minimize effect of turbulent flow around the jet, the

atomizer was placed at the center of a custom flow straightener. Air flow rate was monitored using a thermal mass flow meter (4043, TSI, Shoreview, MN, USA) which was accurate to 2% of the reading. Air temperature and relative humidity were monitored constantly using a hygrometer (HUMICAP® HM70, Vaisala, Helsinki, Finland). Accuracy of humidity measurement was ±1 %RH between +15 and +25 °C. Accuracy of temperature measurement was ±0.2 °C at +20 °C. Relative humidity of the air was always kept below 4% to avoid icing of the water vapor at the orifice due to the evaporative cooling effect of the volatile liquid. Air temperature was in 20.0±2.0 °C range.

4.3 RESULTS AND DISCUSSION

Figure 4-5 shows images taken from non-flashing and flashing jets. The non-flashing jet in the left panel was characterized as being steady and thin. On the other hand, the flashing jet was observed to be expanded and unsteady. For each jet diameter and propellant composition, jets were observed to be flashing above a certain temperature and ceased flashing below this temperature. Alternatively, for a given temperature, a jet diameter could be assigned above which jets were in flashing mode and below which flashing did not occur. This jet diameter was termed the critical jet diameter.
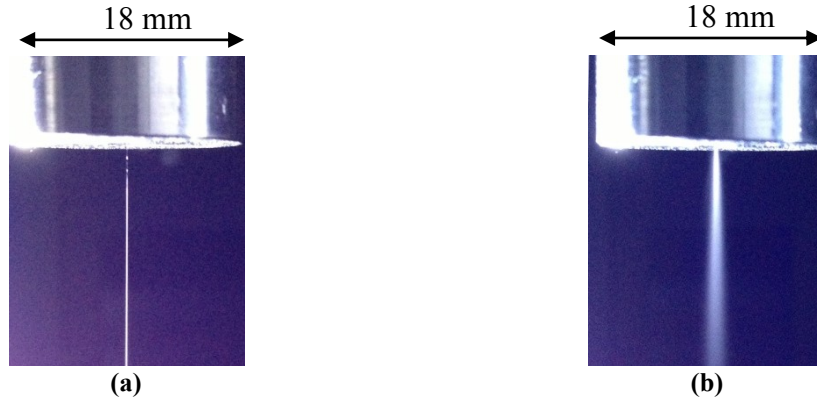
Figure 4-5: Images taken from HFA134a jets: **(a)** thin stable jet below critical temperature, **(b)** expanded unstable spray above critical temperature

Figure 4-6 and Figure 4-7 show the critical jet diameter, d_j, versus initial jet temperature, for formulations containing propellants HFA134a, and HFA227ea respectively. It is apparent that for each formulation the critical jet diameter varied inversely with the initial propellant temperature.

The addition of ethanol increased the critical jet diameter for each temperature regardless of the choice of propellant, i.e., it impeded flash atomization, as can be seen in both Figure 4-6 and Figure 4-7.
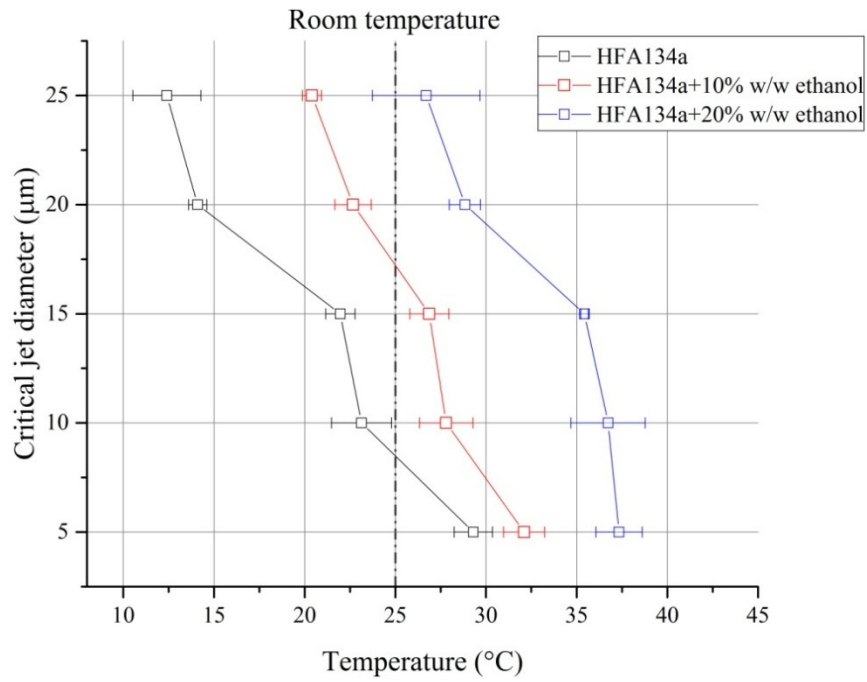
Figure 4-6 Critical jet diameter (assuming jet diameter equals orifice diameter) depicted versus critical initial jet temperature for mixtures containing HFA134a (n=3).
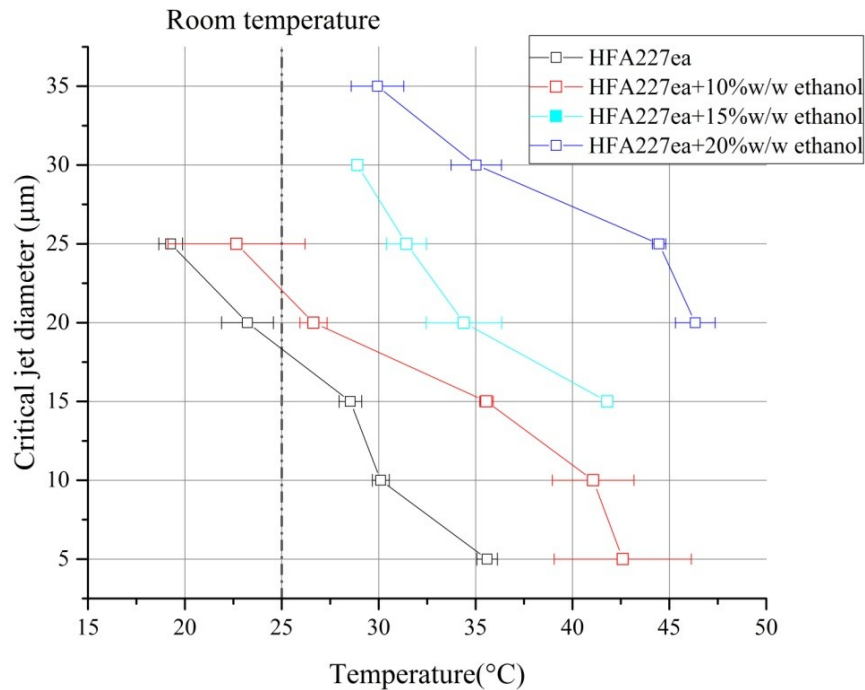
Figure 4-7 Critical jet diameter (assuming jet diameter equals orifice diameter) depicted versus critical initial jet temperature for mixtures containing HFA227ea (n=3).

Figure 4-6 shows that for formulations containing HFA134a propellant at room temperature, critical jet diameters of about 10 and 15 μm were observed for the cases without ethanol and 10% w/w ethanol, respectively. For formulations with HFA227ea at room temperature, Figure 4-7 shows that critical jet diameters of about 18 and 22 μm were observed for the cases without ethanol and 10% w/w ethanol, respectively. For both HFA134a and HFA227ea, concentrations of ethanol higher than 10% w/w prevented flash atomization at room temperature in our experiments.

Comparison of Figure 4-6 and Figure 4-7 reveals the effect of propellant type on critical jet diameter at identical ethanol concentrations. It can be seen that for all our formulations, HFA134a propellant initiates flash atomization at a smaller critical jet

diameter than HFA227ea formulations at the same temperatures. This effect can be attributed to the higher vapor pressure and enthalpy of evaporation of HFA134a than HFA227ea at similar temperatures. Vapor pressure affects flash atomization in two different ways: via evaporative cooling rate and via bubble growth rate. These two competing effects both increase at increased vapor pressures. The results shown in Figure 4-6 and Figure 4-7 imply that increasing the vapor pressure through propellant selection has a higher effect on bubble growth than evaporative cooling.

To determine the effect of jet velocity on the atomization event in the droplet chain, two settings were tested at different head space pressures to examine the effect of velocity change on the mode of atomization. The details of the data acquired are shown in Table 4-3. In the tested range of velocity change, the jet velocity did not affect the onset of flash atomization, which indicates that shear forces or aerodynamic forces on the jet do not affect jet disintegration. This finding parallels that of Tamaki et al. [102] who found the effect of interfacial forces on the disintegration of the jet was negligible. A 50% increase in head space pressure as reported in Table 4-3 is expected to be equivalent to a 22% increase in jet velocity according to Bernoulli's relation. Due to its lack of effect, jet velocity was not included in the dimensional analysis shown below.

Note that at higher velocities it may be expected that the jet evaporative cooling could be affected by the high speed motion of the air around the jet. Also, at higher velocities, jet turbulence itself can impose high pressure fluctuations in the liquid phase and create more vapor bubbles and accelerate the flash atomization event [27].

82

Table 4-3 Dataset acquired for testing the effect of jet velocity on critical temperature required for flash atomization of the jet (n=3)

Concentration of Ethanol in HFA227ea (w/w)	Head space pressure (bar)	Orifice diameter (μm)	critical temperature (Mean±SD*) (°C)
10	12	10	41.1±2.1
10	18	10	42.9±2.6
15	12	20	34.4±1.9
15	18	20	34.7±2.1

*Standard deviation

4.3.1 Dimensional analysis

A dimensional analysis was conducted following Kundu et al. [103] and Ivey et al. [5]. Nine different properties were assumed to play a role in the onset of flash atomization in a cylindrical jet. The list of these parameters, the reason for choosing them, and their range of change in the experimental data set are listed in Table 4-4.

Although the liquid phase viscosity appears in the Rayleigh-Plesset equation, it was not used here for data analysis, because the liquid viscosity term did not appear in any of the analytical solutions for bubble growth; inertia-controlled growth, or diffusion-controlled growth [50]. Choosing the four repeating variables as d_j, ρ_L, T, p_{sat}, the following dimensionless groups are obtained:

$$\Pi_1 = \frac{\rho_g}{\rho_L} \tag{4-5}$$

$$\Pi_2 = \frac{\rho_L c_{pL}(T - T_{sat})}{p_{sat}} \tag{4-6}$$

$$\Pi_3 = \frac{T_{sat}}{T - T_{sat}} \tag{4-7}$$

$$\Pi_4 = \frac{\sigma}{p_{sat}\, d_j} \tag{4-8}$$

$$\Pi_5 = \frac{\rho_L \Delta H_v}{p_{sat}} \tag{4-9}$$

$$\Pi_6 = \frac{\alpha_L^2 \rho_L}{p_{sat} d_j^2} \tag{4-10}$$

To calculate the values of the dimensionless groups in equations (4-5)-(4-10), many

thermo-physical properties of the mixtures must be known. All the temperature

dependent properties and the liquid temperature itself are calculated at the average

temperature of the initial jet temperature, T, and the saturation temperature of the liquid

at ambient pressure, T_{sat}.

Table 4-4 List of the properties included in the nondimensionalization process, the reason for considering them and their ranges of changes. Refer to nomenclature for unit of each parameter.

Variable	Symbol	Reasons for inclusion in analysis		Mean ± SD[*]	RSD[×]
Critical jet diameter	d_j	Dependent variable		N.A.	N.A.
Saturation pressure	p_{sat}	Driving force for bubble expansion during flash atomization		2.80×10^5 $\pm 4.01 \times 10^4$	14.35%
Surface tension of liquid propellant in air	σ	Impedes incipient bubble growth rate according to Rayleigh-Plesset equation [50]		11.5×10^{-3} $\pm 1.6 \times 10^{-3}$	13.5%
Specific heat capacity of liquid phase	c_{pL}	Affects the heat content available in the liquid phase for bubble growth and flash atomization		1.35×10^3 ± 128	9.50%
Degree of superheat of the liquid phase	$T - T_{sat}$	Determines the amount of sensible heat available for bubble growth during flash evaporation		25.5 ± 3.85	15.1%
Saturation temperature of the formulation at ambient pressure	T_{sat}	Flash evaporation cannot occur below this temperature.	HFA134a mixtures	$-26.1°C$	N.A.
			HFA227ea mixtures	$-16.5°C$	
Enthalpy of evaporation of the mixture	ΔH_v	Affects the amount of heat lost during evaporative cooling (both internal evaporation and external evaporation)	HFA134a mixtures	1.98×10^5 $\pm 2.83 \times 10^3$	1.42%
			HFA227ea mixtures	1.20×10^5 $\pm 1.98 \times 10^3$	1.66%
Density of the gas phase	ρ_g	Affects bubble growth rate		18.7 ± 4.28	22.8%
Density of the liquid phase	ρ_L	Affects bubble growth rate		1.29×10^3 ± 97.4	7.56%
Thermal diffusivity of the liquid phase	$\alpha_L = \dfrac{k_L}{\rho_L c_{pL}}$	Determines how rapidly evaporative cooling at the surface cools down the jet.		5.04×10^{-8} $\pm 7.23 \times 10^{-9}$	14.3%

*Standard deviation
×Relative standard deviation

To calculate surface tension, σ, liquid specific heat capacity, c_{pL}, and liquid thermal

conductivity, k_L, of the mixtures, mass fraction weighted averages of those properties of

propellants and ethanol were calculated. To calculate liquid density of the mixture, ρ_L, equation (4-11) was used.

$$\frac{1}{\rho_L} = \frac{Y_{HFA}}{\rho_{L,HFA}(\bar{T})} + \frac{Y_{eth}}{\rho_{L,eth}(\bar{T})} \qquad (4\text{-}11)$$

It was assumed that the vapor pressure of the mixture was not affected by the presence of ethanol at the tested concentrations [104]. The gas density, ρ_g, saturation pressure, p_{sat}, saturation temperature, T_{sat}, and enthalpy of evaporation, ΔH_v, of the pure propellants were used for the mixtures.

Calculated mean values and standard deviations of all dimensionless groups are listed in Table 4-5.

Table 4-5 List of dimensionless groups used for dimensional analysis

Dimensionless group	Mean ± Standard Deviation	RSD
Π_1	0.0146 ± 0.0033	22.7%
Π_2	157 ± 4.8	3.1%
Π_3	10.3 ± 1.6	16.0%
Π_4	0.0031 ± 0.0018	59.2%
Π_5	721 ± 182	25.3%
Π_6	$9.99 \times 10^{-8} \pm 1.39 \times 10^{-7}$	139.2%

Π_2 was not considered further, because, as Table 4-5 shows, Π_2 remains nearly constant in the current data set in spite of large changes in heat capacity of the liquid phase and saturation pressure. The following correlation between the dimensional groups had high coefficients of determination:

$$\Pi_6 = 9.1761 \times 10^{-3}\Pi_4^2 - 0.0072 \times 10^{-3}\Pi_4, \ R^2 = 0.9982 \tag{4-12}$$

Inserting the material properties yields:

$$d_j = 1274\frac{\sigma}{p_{sat}} - 139 \times 10^3 \frac{\alpha_L^2 \rho_L}{\sigma} \tag{4-13}$$

Equation (4-12) and the dimensionless data acquired in the tests are depicted in Figure 4-8.
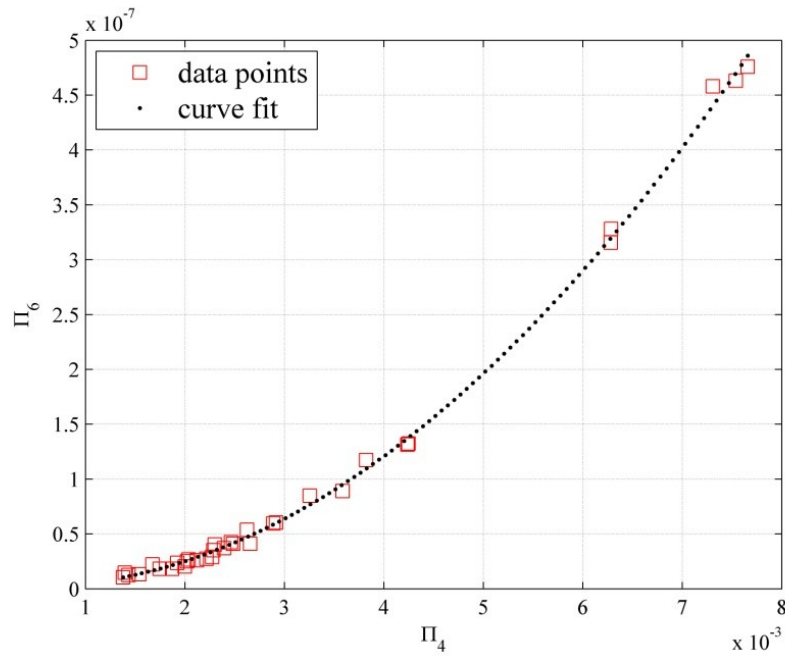
Figure 4-8 Plot of $\boldsymbol{\Pi_6}$ versus $\boldsymbol{\Pi_4}$ using a quadratic curve fit

The first term in the right hand side of equation (4-13) is similar to the correlation developed by Ivey et al.[5] for the content equivalent diameter, d_c, of particles emitted from solution metered dose inhalers:

$$d_c = 416 \frac{\sigma}{p_{sat}}$$ (4-14)

Both equations (4-13) and (4-14) predict that a decrease in surface tension or an increase in vapor pressure lead to production of finer jets or smaller droplets, respectively. Both correlations predict quite similar diameters, which is interesting given that the nozzle used here is different than the ones used in pressurized metered dose inhalers studied in Ivey et al.'s work [5]. However, in our experiments we find that the thermal conductivity of the liquid phase also affects the critical jet diameter, in agreement with the work of Mutair and Ikegami [105] who showed that the evaporation of superheated droplets was greatly affected by heat conduction in the liquid phase. Both terms in the right hand side of equation (4-13) have the same order of magnitude which further emphasizes the importance of thermal diffusivity in determining the critical jet diameter. The negative sign of the thermal diffusivity term suggests that the heat flow inside the droplet preferentially provides more heat for internal evaporation and bubble growth than is supplied for external evaporation. This finding indicates that flash atomization could be enhanced by using liquids (either propellants or co-solvents) with high thermal diffusivities.

Nomenclature

c_{pL}	Specific heat capacity of liquid $\left[\frac{J}{kg.K}\right]$
d_c	Content equivalent diameter [m]
d_d	Droplet diameter [m]
d_j	Jet diameter [m]
ΔH_v	Enthalpy of evaporation $\left[\frac{J}{kg}\right]$
Ja	Dimensionless Jakob number
k_L	Thermal conductivity of the liquid phase $\left[\frac{W}{m.\,K}\right]$
M	Molecular weight $\left[\frac{kg}{mol}\right]$
p_{sat}	Saturation pressure [Pa]
R	Ideal gas constant $\left[\frac{J}{mol.K}\right]$
T	Temperature [K]
T_{amb}	Ambient temperature [K]
T_b	Boiling point temperature [K]
T_{sat}	Saturation temperature [K]
T_{wb}	Wet bulb temperature of the droplet [K]
$\bar{T}$	Average temperature [K]
We	Dimensionless Weber number
Y	Mass fraction
α_L	Liquid thermal diffusivity $\left[\frac{m^2}{s}\right]$
ρ_g	Vapor density $\left[\frac{kg}{m^3}\right]$
ρ_L	Liquid density $\left[\frac{kg}{m^3}\right]$
σ	Liquid-vapor surface tension $\left[\frac{N}{m}\right]$
ϕ	Correction factor

Chapter 5. Conclusions

Effect of environmental conditions on the efficiency of the metered dose inhalers was discussed in Chapter 2. The delivery of pMDI formulations into the lung is affected by environmental conditions, and there are differences in the delivery of these formulations, depending on solution or suspension formulation, or the presence of excipients. While all three tested formulations were weakly affected by air flow rate, relative humidity affected lung delivery of the suspension more strongly than the solutions. On the other hand, temperature affected lung delivery of the solutions but had generally no effect on the suspension.

Residual dry particles after propellant evaporation are subject to condensation; however, the importance of this effect is apparently formulation dependent, possibly being affected by plume temperature and the number of emitted particles. At 20°C, these effects of relative humidity are relatively minor, but at 40°C can result in doubling of mouth-throat dose, with concomitant reduction in lung delivery. Awareness of such effects of environmental conditions may be useful during design, testing and usage of pMDIs.

In Chapter 3 design of a new atomizer capable of producing monodisperse droplets from high vapor pressure liquids such as HFA227ea and HFA134a was discussed.

Generation of monodisperse droplets from such fluids is useful for future fundamental exploration of the evaporation and particle formation from metered dose inhaler (MDI) sprays for pharmaceutical applications. Monodispersity of the droplets allows for the quantitative study of the behavior of the droplets. High vapor pressures of such liquids cause flash atomization at typical room temperatures and conditions, subsequently producing a wide range of droplet sizes and making it impossible for existing monodisperse aerosol generators to produce monodisperse droplets from these liquids. The atomizer presented here benefits from a thinner piezoelectric transducer to apply the controlled capillary wave disturbance to the emerging jet of propellant, incorporated with a newly designed high pressure feed line and a built-in circuit for cooling of the jet. With the current assembly, there exists the potential for examining MDI particle formation from solutions composed of mixtures of propellants and the production of dry particles from any propellant-soluble compound. Such a tool is expected to be useful in advancing our understanding of the rather complex particle formation process that occurs with MDI sprays, and moving forward with novel MDI formulations and designs.

In Chapter four, parameters controlling flash atomization in micro-jets were explored the. Three parameters affecting the onset of flash atomization in a propellant jet were investigated: jet diameter, initial jet temperature, and propellant mixture. By manipulating these three parameters it was possible to control the onset of flash atomization event in the micro-jet.

91

It was observed that a critical jet diameter existed above which the jet disintegrated due to flash atomization. The critical jet diameter was affected by the jet initial temperature and formulation. Lowering the jet initial temperature as well as the addition of ethanol always increased the critical jet diameter. Jets produced with HFA134a propellant rather than HFA227ea had lower critical jet diameters. Varying the velocity of the jet did not affect the onset of flash atomization event and suggests that air shear did not play a dominant role in determining the critical jet diameter.

A correlation was proposed relating the critical jet diameter to propellant vapor pressure, liquid-vapor surface tension as well as mixture liquid density and heat diffusivity. The magnitude and trend of change of critical jet diameter was similar to that seen with content equivalent diameter proposed by previous researchers for pMDIs [5].

Knowledge of the parameters controlling flash atomization may be of use in producing finer droplet size distributions or in controlling the size distribution of the initial droplets produced in metered dose inhaler plumes. However, the atomization process in actual metered dose inhalers is a more complicated process because of the use of twin serial orifices, the existence of an expansion chamber between the two, and the transient nature of the process. However, the findings of this study may be useful in understanding the general trends of change due to variations in the influential parameters.

APPENDIX-A: THERMO-PHYSICAL PROPERTIES OF HFA134A, HFA227EA, AND ETHANOL

Table A-1 Molar masses and critical temperatures of HFA134a, HFA227ea and ethanol

Liquid	Molar mass $\left[\frac{kg}{mol}\right]$	Critical temperature [K]
HFA134a	102.032×10^{-3}	374.1
HFA227ea	170.03×10^{-3}	375.95
Ethanol	46.07×10^{-3}	N.A.

Table A-2 Thermo-physical properties of HFA134a, HFA227ea and ethanol

Property, Equation, Units		Coefficients	Reference
Liquid phase specific heat capacity: $$c_{pL} = [A + BT + CT^2 + DT^3 + ET^4 + FT^5]/M$$ T is in [K]. c_{pL} is in $\left[\frac{J}{kg.K}\right]$.	HFA134a	A=-2.04E3 B=47.5 C=-0.413 D=1.77E-03 E=-3.76E-06 F=3.16E-09	[106]
	HFA227ea	A=-1.61E03 B=42.1 C=-0.391 D=1.78E-03 E=-3.95E-06 F=3.44E-09	[106]
	Ethanol	A=4.23E03 B=-63.6 C=0.383 D=-1.14E-03 E=1.69E-06 F= -1.01E-09	[106]

Property, Equation, Units		Coefficients	Reference
Saturation pressure: $$p_{\text{sat}} = 1 \times 10^5 \exp\left(A + \frac{B}{C+T} + DT + E\log(T)\right)$$ T is in [K]. p_{sat} is in [Pa].	HFA134a	A=103 B=-5.24E3 C=0 D=0.024 E=-15.8	[25]
	HFA227ea	A=126 B=-5.95E3 C=0 D=0.031 E=-20.0	[26]
Liquid Thermal conductivity: $k_{\text{L}} = A + BT + CT^2 + DT^3 + ET^4 + FT^5$ T is in [K]. k_{L} is in $\left[\frac{W}{\text{m. K}}\right]$.	HFA134a	A=0.322 B=-1.78E-03 C=7.13E-06 D=-2.25E-08 E=4.31E-11 F=-3.72E-14	[106]
	HFA227ea	A=7.39E-02 B=5.66E-04 C=-4.79E-06 D=1.65E-08 E=-3.35E-11 F=2.95E-14	[106]
$k_{\text{L}} = A + BT + CT^2$ T is in [K]. k_{L} is in $\left[\frac{W}{\text{m. K}}\right]$.	Ethanol	A=0.225 B=-5.63E-05 C=-4.22E-07	[107]
Liquid density: $$X = \sqrt[3]{1 - \left(\frac{T}{T_{\text{c}}}\right)}$$ $\rho_{\text{L}} = 1000 \times [A + BX + CX^2 + DX^3 + EX^4]$ T is in [K]. ρ_{L} is in $\left[\frac{\text{kg}}{\text{m}^3}\right]$.	HFA134a	A=508 B=968 C=298 D=79.9 E=89.8	[25]
	HFA227ea	A=580 B=1.06E3 C=778 D=-852 E=708	[26]

Property, Equation, Units		Coefficients	Reference
$X = 1 + \left(1 - \dfrac{T}{C}\right)^{D}$ $\rho_{\mathrm{L}} = \left[\dfrac{A}{B^{X}}\right] \times M$ T is in [K]. ρ_{L} is in $\left[\dfrac{\mathrm{kg}}{\mathrm{m}^{3}}\right]$.	Ethanol	A=1.63 B=0.275 C=514 D=0.232	[108]
Vapor density: $p = [A + BT + CT^{2} + DT^{3} + ET^{4} + FT^{5}]$ $\rho_{\mathrm{g}} = 1000 \times 10^{p} \times M$ T is in [K]. ρ_{g} is in $\left[\dfrac{\mathrm{kg}}{\mathrm{m}^{3}}\right]$.	HFA134a	A=-70.4 B=1.18 C=-0.009 D=3.18E-05 E=-5.96E-08 F=4.47E-11	[106]
	HFA227ea	A=-50.7 B=0.773 C=-0.005 D=1.90E-05 E=-3.52E-08 F=2.63E-11	[106]
Enthalpy of evaporation: $X = \sqrt[3]{1 - \left(\dfrac{T}{T_{\mathrm{c}}}\right)}$ $\Delta H_{\mathrm{v}} = 1000 \times [A + BX + CX^{2} + DX^{3} + EX^{4}]$ T is in [K]. ΔH_{v} is in $\left[\dfrac{\mathrm{J}}{\mathrm{kg}}\right]$.	HFA134a	A=0 B=164 C=460 D=-511 E=219	[25]
	HFA227ea	A=64.0 B=-273 C=1.07E3 D=-1.01E3 E=353	[26]

Property, Equation, Units		Coefficients	Reference
Surface tension: $$\sigma = 0.001 \times A\left(1 - \frac{T}{T_c}\right)^{1.26}$$ T is in [K]. σ is in $\left[\frac{N}{m}\right]$.	HFA134a	A=60.2	[25]
	HFA227ea	A=50.5	[26]
$\sigma = A + BT + CT^2 + DT^3 + ET^4 + FT^5$ T is in [K]. σ is in $\left[\frac{N}{m}\right]$.	Ethanol	A=0.009 B=0.001 C= -4.75E-06 D=1.38E-08 E=-1.96E-11 F=1.11E-14	[106]

Appendix-B:Design drawings of the atomizer components
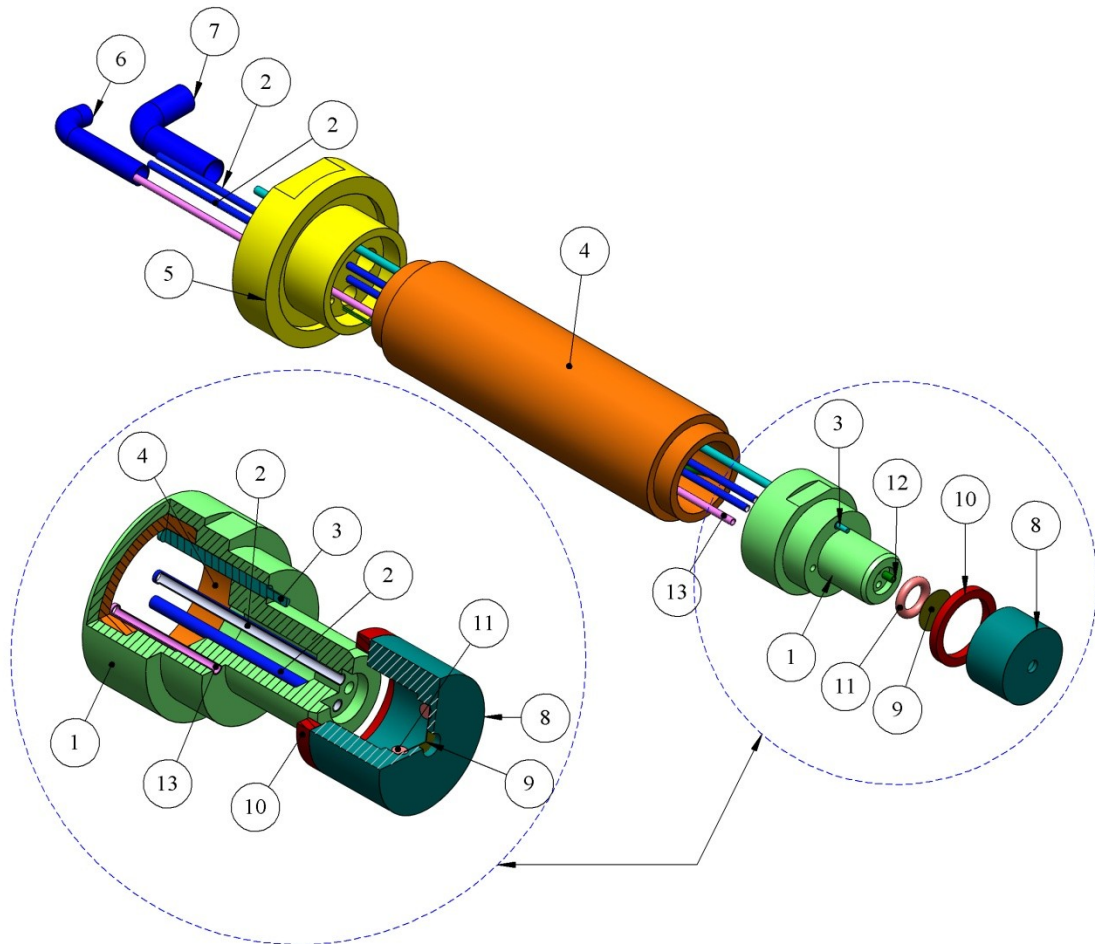
part #	part name	note
1	feed nozzle	
2	hypoedermic tube	used to deliver and drain solution
3	spring probe	Mouser #: 565-6354
4	atomizer body	
5	base	
6	3/16" tube	
7	1/4" tube	
8	dispersion cup	
9	orifice plate	Edmund Optics pinholes
10	piezo ceramic	Pz26 from Ferroperm
11	O-ring	EPDM
12	thermocouple	
13	hypodermic tube	used for dispersion

B-1 Atomizer assembly and name of individual parts

NOTES: (UNLESS OTHERWISE SPECIFIED)

1. ALL DIMENSIONS IN MILLIMETERS
2. PART HAS TO BE CLEAN AND BURR FREE

0
5
85
90

Ø17
Ø21
Ø25

UNLESS OTHERWISE NOTED		NAME	DATE	Particle Engineering Lab		
DIMENSIONAL TOLERANCES: FRAC.: ± ANG.: ± DEC. (.xx): ± DEC. (.xxx): ±	DRAWN			TITLE Atomizer Body		
	ENG.					
	CHECKED					
	APPROVED					
MATERIAL				A	DRAWING NUMBER	REV
NEXT ASSY.	NO. REQD.					
DO NOT SCALE DRAWINGS				SCALE 1:1	WEIGHT	SHEET 1 of 1

5   4   3   2   1

B-2 Drawing of atomizer body. Its main use is to act as a shell to contain thermostatic liquid around the hypodermic feed tubing and adjust the temperature of the feed.
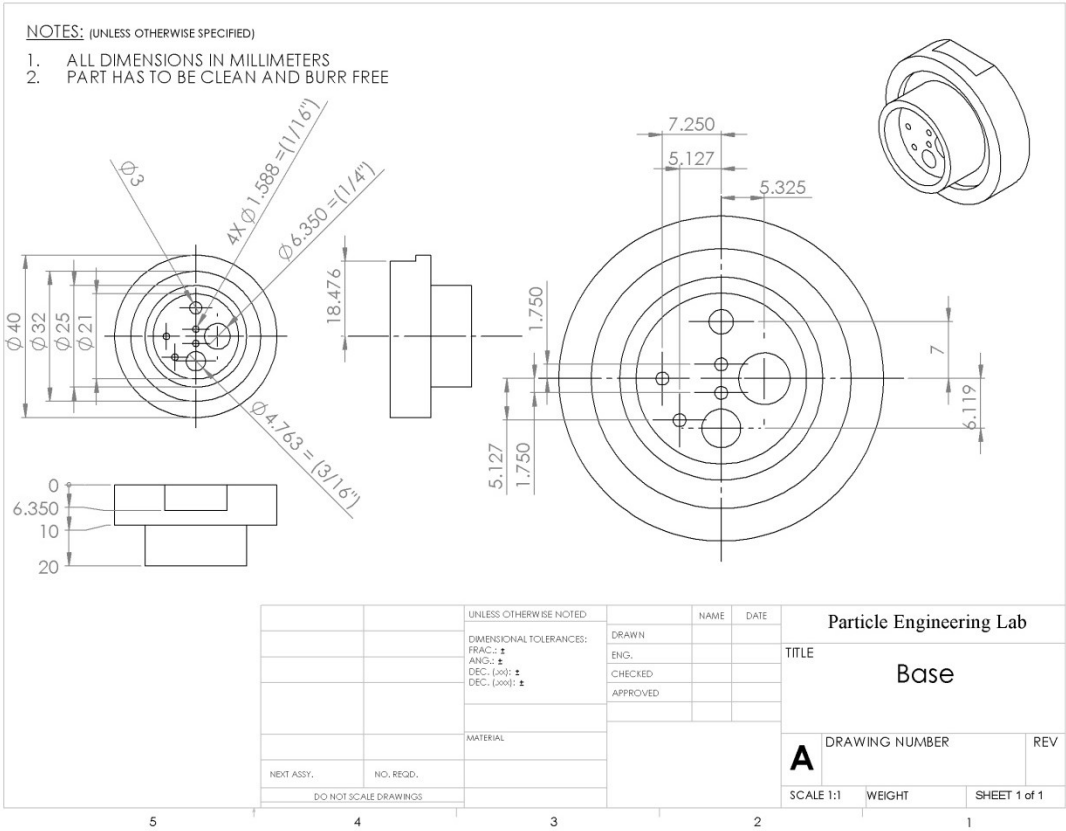
B-3 Drawing of the base of the atomizer.

NOTES: (UNLESS OTHERWISE SPECIFIED)

1. ALL DIMENSIONS IN MILLIMETERS
2. PART HAS TO BE CLEAN AND BURR FREE
3. Two holes are revmoved from the previous drawing. They should be blocked.
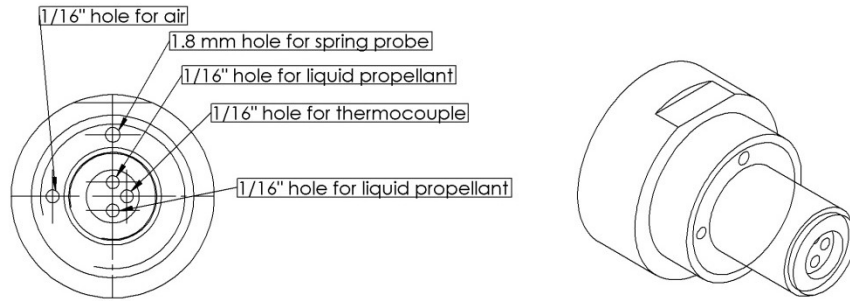
1/16" hole for air
1.8 mm hole for spring probe
1/16" hole for liquid propellant
1/16" hole for thermocouple
1/16" hole for liquid propellant

		UNLESS OTHERWISE NOTED		NAME	DATE	Particle Engineering Lab	
		DIMENSIONAL TOLERANCES: FRAC.: ± ANG.: ± DEC. (.xx): ± DEC. (.xxx): ±	DRAWN			TITLE **Feed Nozzle Description**	
			ENG.				
			CHECKED				
			APPROVED				
		MATERIAL				A	DRAWING NUMBER / REV
NEXT ASSY.	NO. REQD.					SCALE 2:1	WEIGHT / SHEET 1 of 1
DO NOT SCALE DRAWINGS							

5   4   3   2   1

B-4 Explanation of the purpose of each hole in the feed nozzle.

B-5 Feed nozzle drawing

NOTES: (UNLESS OTHERWISE SPECIFIED)

1. ALL DIMENSIONS IN MILLIMETERS
2. PART HAS TO BE CLEAN AND BURR FREE

Ø3

Ø18

A
A

11
10
8
7

M14X1.4

SECTION A-A

UNLESS OTHERWISE NOTED		NAME	DATE	Particle Engineering Lab		
DIMENSIONAL TOLERANCES: FRAC.: ± ANG.: ± DEC. (.xx): ± DEC. (.xxx): ±	DRAWN					
	ENG.			TITLE		
	CHECKED					
	APPROVED			Orifice Cup		
MATERIAL				A	DRAWING NUMBER	REV
NEXT ASSY.	NO. REQD.			SCALE 2:1	WEIGHT	SHEET 1 of 1
DO NOT SCALE DRAWINGS						
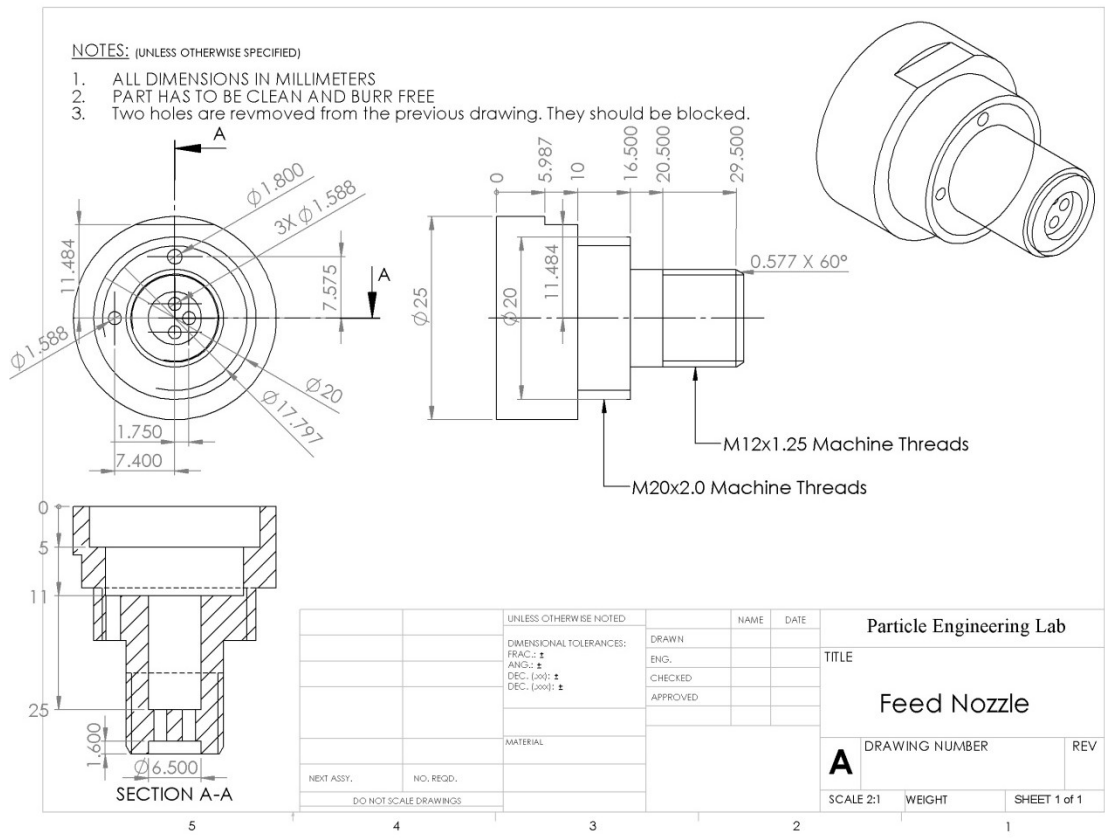
B-6 Orifice cup drawing. It is designed in such a way that it can handle high pressures when finger-tight on the feed nozzle.

103
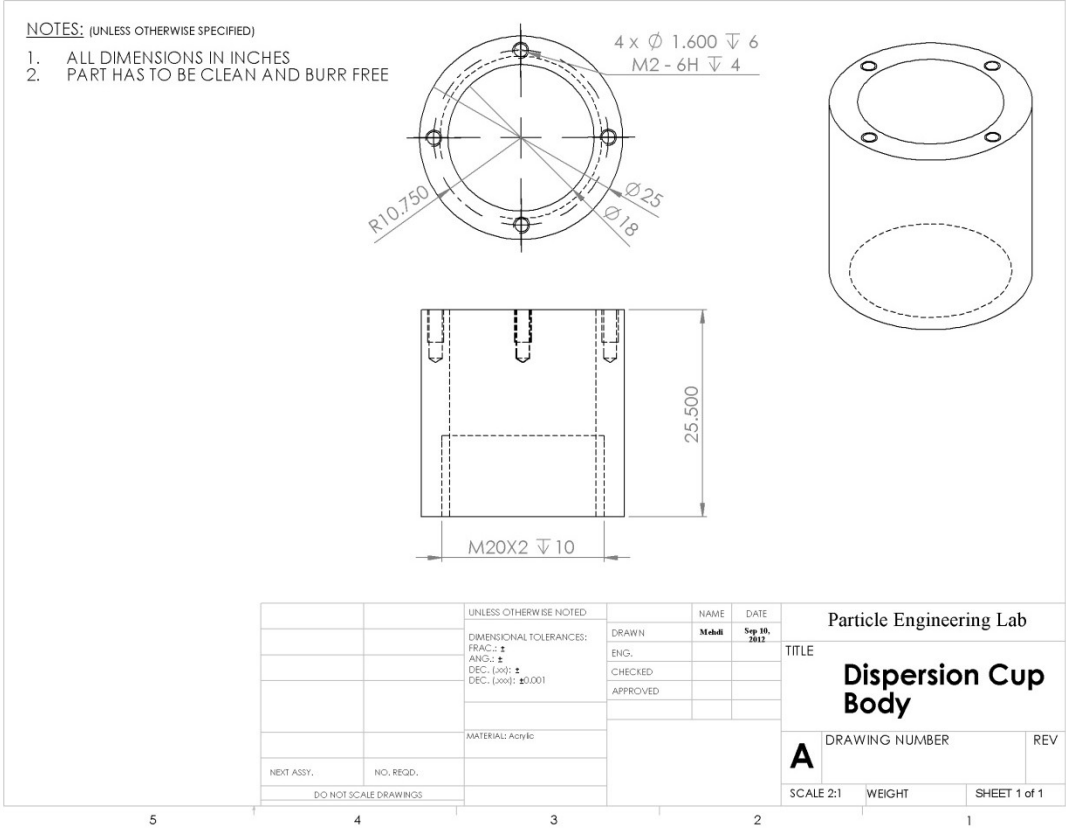
B-7 Drawing of dispersion cup body. Dispersion cup has two separate components: body and top. By separating the two it is possible to use this cup for different applications like charging the droplets.

B-8 Drawing of dispersion cup top.

Bibliography

1.   Kaur, R., et al., *Advanced aerosol delivery devices for potential cure of acute and chronic diseases*. Crit Rev Ther Drug Carrier Syst, 2014. **31**(6): p. 495-530.

2.   Lavorini, F. and G.A. Fontana, *Targeting drugs to the airways: The role of spacer devices*. Expert Opin Drug Deliv, 2009. **6**(1): p. 91-102.

3.   Stein, S.W., et al., *Advances in Metered Dose Inhaler Technology: Hardware Development*. AAPS PharmSciTech, 2014. **15**(2): p. 326-338.

4.   Newman, S. and P. Anderson, *Respiratory drug delivery : essential theory and practice*. xxvi, 388 pages.
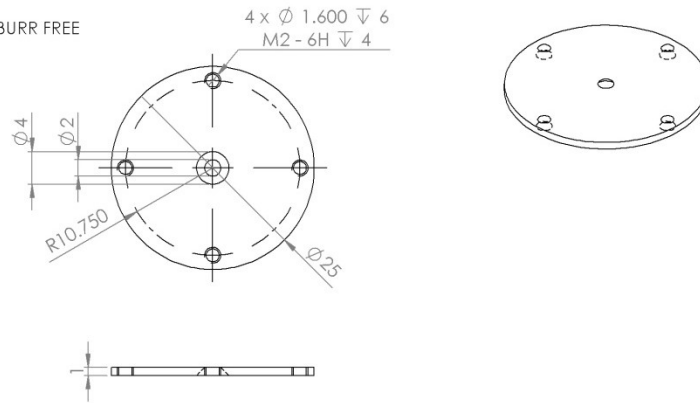
5.   Ivey, J.W., et al., *A correlation equation for the mass median aerodynamic diameter of the aerosol emitted by solution metered dose inhalers*. International Journal of Pharmaceutics, 2014. **465**(1-2): p. 18-24.

6.   Hickey, A.J., *Controlled delivery of inhaled therapeutic agents*. J Control Release, 2014. **190**: p. 182-8.

7.   Bisgaard, H., C. O'Callaghan, and G.C. Smaldone, *Drug delivery to the lung*. Lung biology in health and disease2002, New York: M. Dekker. xvi, 511 p., 1 p. of plates.

8.   Hickey, A.J., *Inhalation aerosols : physical and biological basis for therapy*. Lung biology in health and disease1996, New York: M. Dekker. xv, 511 p.

9.   Newman, S.P., *Principles of metered-dose inhaler design*. Respir Care, 2005. **50**(9): p. 1177-90.

10.   Chen, Y., et al., *The influence of actuator materials and nozzle designs on electrostatic charge of pressurised metered dose inhaler (pMDI) formulations*. Pharmaceutical Research, 2014. **31**(5): p. 1325-37.

11.   Smyth, H., et al., *Spray pattern analysis for metered dose inhalers: effect of actuator design*. Pharmaceutical Research, 2006. **23**(7): p. 1591-6.

12.   Lewis, D., *Metered-dose inhalers: actuators old and new*. Expert Opinion on Drug Delivery, 2007. **4**(3): p. 235-245.

13.   Brocklebank, D., et al., *Comparison of the effectiveness of inhaler devices in asthma and chronic obstructive airways disease: a systematic review of the literature*. Health Technol Assess, 2001. **5**(26): p. 1-149.

14.   *Package Leaflet: Information for the user, Fostair 100/6 micrograms per actuation pressurised inhalation solution*, Chiesi.

15.   *PACKAGE LEAFLET: INFORMATION FOR USER: Clenil® Modulite® 50 micrograms per actuation pressurised inhalation solution, beclometasone dipropionate*, Chiesi.

16.   Myrdal, P.B., P. Sheth, and S.W. Stein, *Advances in Metered Dose Inhaler Technology: Formulation Development.* AAPS PharmSciTech, 2014. **15**(2): p. 434-455.

17.   Bell, J. and S. Newman, *The rejuvenated pressurised metered dose inhaler.* Expert Opinion on Drug Delivery, 2007. **4**(3): p. 215-234.

18.   Hochrainer, D., et al., *Comparison of the aerosol velocity and spray duration of Respimat Soft Mist inhaler and pressurized metered dose inhalers.* J Aerosol Med, 2005. **18**(3): p. 273-82.

19.   Versteeg, H.K.H., G.K. . *NEAR-ORIFICE SPRAY AND VALVE FLOW REGIME OF A PHARMACEUTICAL PRESSURISED METERED DOSE INHALER*. in *18th Annual Conference on Liquid Atomization & Spray Systems*. 2002. Zaragoza, SPAIN.

20.   Stein, S.W., *Estimating the number of droplets and drug particles emitted from MDIs.* AAPS PharmSciTech, 2008. **9**(1): p. 112-115.

21.   Stein, S.W., P. Sheth, and P.B. Myrdal, *A model for predicting size distributions delivered from pMDIs with suspended drug.* International Journal of Pharmaceutics, 2012. **422**(1-2): p. 101-15.

22.   Lewis, D.A., *Intrinsic Particle Size Distribution: A New Metric to Guide the Design of HFA Solution pMDIs*, in *Respiratory Drug Delivery Europe* 2013. p. 175-184.

23.   Hinds, W.C., *Aerosol technology : properties, behavior, and measurement of airborne particles*. 2nd ed1999, New York: Wiley. xx, 483 p.

24.   Sheth, P., S.W. Stein, and P.B. Myrdal, *Factors Influencing Aerodynamic Particle Size Distribution of Suspension Pressurized Metered Dose Inhalers.* AAPS PharmSciTech, 2014.

25.   Mexichem UK Limited, *ZEPHEX® 134a: Physical Property Data Sheet SI Units*, 2010: Runcorn, UK.

26.   Mexichem UK Limited, *ZEPHEX® 227ea: Physical Property Data Sheet SI Units*, 2010: Runcorn, UK.

27.   Finlay, W.H., *The mechanics of inhaled pharmaceutical aerosols : an introduction* 2001, San Diego: Academic Press. xi, 306 p.

28.   Fink, J. and A. Ari, *Aerosol delivery to intubated patients.* Expert Opinion on Drug Delivery, 2013. **10**(8): p. 1077-1093.

29.   Ari, A., J.B. Fink, and R. Dhand, *Inhalation Therapy in Patients Receiving Mechanical Ventilation: An Update.* Journal of Aerosol Medicine and Pulmonary Drug Delivery, 2012. **25**(6): p. 319-332.

30.   Vehring, R., *Pharmaceutical particle engineering via spray drying.* Pharmaceutical Research, 2008. **25**(5): p. 999-1022.

31.   Versteeg, H.K., G.K. Hargrave, and M. Kirby, *Internal flow and near-orifice spray visualisations of a model pharmaceutical pressurised Metered Dose Inhaler.* Second International Conference on Optical and Laser Diagnostics, 2006. **45**: p. 207-213.

32.   Martin, A.R., *The effect of humidity on aerosol drug delivery from metered-dose inhalers*, 2004, University of Alberta, 2004. p. [10], 103 leaves.

33.   Golshahi, L., et al., *An In vitro Study on the Deposition of Micrometer-Sized Particles in the Extrathoracic Airways of Adults During Tidal Oral Breathing.* Annals of Biomedical Engineering, 2013. **41**(5): p. 979-989.

34.   Golshahi, L., et al., *In Vitro Correlations for the Estimation of the Deposition of Micrometer-Sized Aerosols in the Oral Airways of Adults and Children during Inhalation of Tidal Breathing Patterns.* Journal of Aerosol Medicine and Pulmonary Drug Delivery, 2013. **26**(2): p. A37-A37.

35.   Golshahi, L. and W.H. Finlay, *An Idealized Child Throat that Mimics Average Pediatric Oropharyngeal Deposition.* Aerosol Science and Technology, 2012. **46**(5): p. I-Iv.

36.   Golshahi, L., M.L. Noga, and W.H. Finlay, *Deposition of inhaled micrometer-sized particles in oropharyngeal airway replicas of children at constant flow rates.* Journal of Aerosol Science, 2012. **49**: p. 21-31.

37.   Rahmatalla, M.F., et al., *In vitro effect of a holding chamber on the mouth-throat deposition of QVAR((R)) (Hydrofluoroalkane-beclomethasone dipropionate).* Journal of Aerosol Medicine-Deposition Clearance and Effects in the Lung, 2002. **15**(4): p. 379-385.

38.   Stein, S.W. and P.B. Myrdal, *A theoretical and experimental analysis of formulation and device parameters affecting solution MDI size distributions.* J Pharm Sci, 2004. **93**(8): p. 2158-75.

39.   Lefebvre, A.H., *Atomization and sprays*. Combustion,1989, New York: Hemisphere Pub. Corp. xi, 421 p.

40.   Anders, K., N. Roth, and A. Frohn, *Operation Characteristics of Vibrating-Orifice Generators - the Coherence Length.* Particle & Particle Systems Characterization, 1992. **9**(1): p. 40-43.

41.   Anders, K., N. Roth, and A. Frohn, *Simultaneous Insitu Measurements of Size and Velocity of Burning Droplets.* Particle & Particle Systems Characterization, 1991. **8**(2): p. 136-141.

42.   Berglund, R.N. and B.Y.H. Liu, *Generation of Monodisperse Aerosol Standards.* Environmental Science & Technology, 1973. **7**(2): p. 147-153.

43. Schneider, J.M. and C.D. Hendricks, *Source of Uniform-Sized Liquid Droplets.* Review of Scientific Instruments, 1964. **35**(10): p. 1349-&.

44. Reitz, R.D., *Atomization and other breakup regimes of a liquid jet*, 1978, Princeton. p. 331 leaves in various pagings.

45. Dumouchel, C., *On the experimental investigation on primary atomization of liquid streams.* Experiments in Fluids, 2008. **45**(3): p. 371-422.

46. Lin, S.P. and R.D. Reitz, *Drop and spray formation from a liquid jet.* Annual Review of Fluid Mechanics, 1998. **30**: p. 85-105.

47. Massoud, M., *Engineering thermofluids : thermodynamics, fluid mechanics, and heat transfer*2005, Berlin: Springer. xxiv, 1119 p.

48. Carey, V.P., *Liquid-vapor phase-change phenomena : an introduction to the thermophysics of vaporization and condensation processes in heat transfer equipment*1992, Washington, D.C.: Hemisphere.

49. Ashgriz, N., *Handbook of atomization and sprays*2011, New York: Springer.

50. Sher, E., T. Bar-Kohany, and A. Rashkovan, *Flash-boiling atomization.* Progress in Energy and Combustion Science, 2008. **34**(4): p. 417-439.

51. Clark, A.R. *Metered atomisation for respiratory drug delivery. [electronic resource]*. 1991.

52. Cleary, V., P. Bowen, and H. Witlox, *Flashing liquid jets and two-phase droplet dispersion I. Experiments for derivation of droplet atomisation correlations.* Journal of Hazardous Materials, 2007. **142**(3): p. 786-796.

53. Kim, C.S., D. Trujillo, and M.A. Sackner, *SIZE ASPECTS OF METERED-DOSE INHALER AEROSOLS.* American Review of Respiratory Disease, 1985. **132**(1): p. 137-142.

54. Mitchell JP, N.M., Wiersema KJ, Doyle CC, and Migunov VA, *The effect of humidification on the size distribution of aerosols delivered to the mechanically ventilated patient.* Journal of Aerosol Medicine, 2003. **16**(2): p. 187-227.

55. Ari, A., H. Areabi, and J.B. Fink, *Evaluation of Aerosol Generator Devices at 3 Locations in Humidified and Non-humidified Circuits During Adult Mechanical Ventilation.* Respiratory Care, 2010. **55**(7): p. 837-844.

56. Lin, H.L., et al., *Influence of Moisture Accumulation in Inline Spacer on Delivery of Aerosol Using Metered-Dose Inhaler During Mechanical Ventilation.* Respiratory Care, 2009. **54**(10): p. 1336-1341.

57. Lange, C.F. and W.H. Finlay, *Overcoming the adverse effect of humidity in aerosol delivery via pressurized metered-dose inhalers during mechanical ventilation.* Am J Respir Crit Care Med, 2000. **161**(5): p. 1614-8.

58. Martin, A.R., D.Y. Kwok, and W.H. Finlay, *Investigating the evaporation of metered-dose inhaler formulations in humid air: Single droplet experiments.* Journal of Aerosol Medicine-Deposition Clearance and Effects in the Lung, 2005. **18**(2): p. 218-224.

59. Martin, A.R. and W.H. Finlay, *The effect of humidity on the size of particles delivered from metered-dose inhalers.* Aerosol Science and Technology, 2005. **39**(4): p. 283-289.

60. Grgic, B., W.H. Finlay, and A.F. Heenan, *Regional aerosol deposition and flow measurements in an idealized mouth and throat.* Journal of Aerosol Science, 2004. **35**(1): p. 21-32.

61. Zhang, Y., K. Gilbertson, and W.H. Finlay, *In vivo-in vitro comparison of deposition in three mouth-throat models with Qvar (R) and Turbuhaler (R) inhalers.* Journal of Aerosol Medicine-Deposition Clearance and Effects in the Lung, 2007. **20**(3): p. 227-235.

62. Zhou, Y., J. Sun, and Y.S. Cheng, *Comparison of Deposition in the USP and Physical Mouth-Throat Models with Solid and Liquid Particles.* J Aerosol Med Pulm Drug Deliv, 2011.

63. Stein, S.W. and P.B. Myrdal, *The relative influence of atomization and evaporation on metered dose inhaler drug delivery efficiency.* Aerosol Science and Technology, 2006. **40**(5): p. 335-347.

64. Williams, R.O. and J. Liu, *Influence of formulation additives on the vapor pressure of hydrofluoroalkane propellants.* International Journal of Pharmaceutics, 1998. **166**(1): p. 99-103.

65. Brambilla, G., et al., *Plume temperature emitted from metered dose inhalers.* International Journal of Pharmaceutics, 2011. **405**(1-2): p. 9-15.

66. *Flixotide™ 125 micrograms Evohaler™, Flixotide™ 250 micrograms Evohaler™ Package Leaflet: Information for the User*, 2011, Allen & Hanburys, Uxbridge, UK.

67. *Qvar® 50 & 100 Autohaler® Beclometasone Dipropionate Package Leaflet: Information for the User*, 2011, Teva UK Ltd., London, UK.

68. Dunbar, C.A., A.P. Watkins, and J.F. Miller, *An experimental investigation of the spray issued from a pMDI using laser diagnostic techniques.* Journal of Aerosol Medicine-Deposition Clearance and Effects in the Lung, 1997. **10**(4): p. 351-368.

69. Clark, A.R., *MDIs: Physics of aerosol formation.* Journal of Aerosol Medicine-Deposition Clearance and Effects in the Lung, 1996. **9**: p. S19-S26.

70. Liu, X.F., W.H. Doub, and C.N. Guo, *Evaluation of metered dose inhaler spray velocities using Phase Doppler Anemometry (PDA).* International Journal of Pharmaceutics, 2012. **423**(2): p. 235-239.

71. Kanig, J.L., *Pharmaceutical aerosols.* Journal of Pharmaceutical Sciences, 1963. **52**(6): p. 513-535.

72. Vehring, R., W.R. Foss, and D. Lechuga-Ballesteros, *Particle formation in spray drying.* Journal of Aerosol Science, 2007. **38**: p. 728-746.

73. Marjamäki, M., et al., *Performance Evaluation of the Electrical Low-pressure Impactor (ELPI).* Journal of Aerosol Science, 2000. **31**: p. 249-261.

74. Zhou, Y., J. Sun, and Y.S. Cheng, *Comparison of deposition in the USP and physical mouth-throat models with solid and liquid particles.* Journal of Aerosol Medicine and Pulmonary Drug Delivery, 2011. **24**: p. 277-284.

75. Japuntich, D., J.I.T. Stenhouse, and B.Y.H. Liu, *A monodisperse aerosol generator for high concentrations of 0.5 to 5 μm solid particles.* Journal of Aerosol Science, 1992. **23, Supplement 1**(0): p. 177-180.

76. Tu, K.-W., *A condensation aerosol generator system for monodisperse aerosols of different physicochemical properties.* Journal of Aerosol Science, 1982. **13**(5): p. 363-371.

77. Lind, T., S. Danner, and S. Guentay, *Monodisperse fine aerosol generation using fluidized bed.* Powder Technology, 2010. **199**: p. 232-237.

78. Mitchell, J.P., *The production of aerosols from aqueous solutions using the spinning top generator.* Journal of aerosol Science, 1984. **15**(1): p. 35-45.

79. Woodcock, A., *The president speaks: prevention is best: lessons from protecting the ozone layer.* Thorax, 2012. **67**(12): p. 1028-31.

80. Rayleigh, L., *On The Instability Of Jets.* Proceedings of the London Mathematical Society, 1878. **s1-10**(1): p. 4-13.

81. Stein, S.W. and P.B. Myrdal, *A theoretical and experimental analysis of formulation and device parameters affecting solution MDI size distributions.* Journal of pharmaceutical sciences, 2004. **93**: p. 2158-75.

82. Rayleigh, L., *On the instability of jets.* Proceedings of London Mathematical Society, 1879. **10**: p. 3-14.

83. Bogy, D.B., *Drop formation in a circular liquid jet.* Annual Review of Fluid Mechanics, 1979. **11**: p. 207-228.

84. Sirignano, W.A. and C. Mehring, *Review of theory of distortion and disintegration of liquid streams.* Progress in energy and combustion science, 2000. **26**: p. 609-655.

85.   Ltd Apc, I., *Piezoelectric Ceramics: Principles and Applications*2011: Apc International, Limited.

86.   Xu, R., *Particle characterization: light scattering methods*. Vol. 13. 2001: Springer.

87.   Hecht, E., *Optics*2002: Addison-Wesley Longman, Incorporated.

88.   Dunbar, C.A., *Atomization mechanisms of the pressurized metered dose inhaler.* Particulate Science and Technology, 1997. **15**(3): p. 195-216.

89.   Clark., A.R., *The Physics of Aerosol Formation by MDIs - Limitations of the Current Approach.* Journal of Biopharmaceutical Sciences, 1992. **3**(1): p. 8.

90.   Shepherd, J.E. and B. Sturtevant, *Rapid Evaporation at the Superheat Limit.* Journal of Fluid Mechanics, 1982. **121**(Aug): p. 379-402.

91.   Park, H.C., K.T. Byun, and H.Y. Kwak, *Explosive boiling of liquid droplets at their superheat limits.* Chemical Engineering Science, 2005. **60**(7): p. 1809-1821.

92.   Shusser, M. and D. Weihs, *Explosive boiling of a liquid droplet.* International Journal of Multiphase Flow, 1999. **25**(8): p. 1561-1573.

93.   Shusser, M. and D. Weihs, *Stability of rapidly evaporating droplets and liquid shells.* International Journal of Multiphase Flow, 2001. **27**(2): p. 299-345.

94.   Kolev, N.I., *Multiphase flow dynamics*. 4th ed2011, Berlin: Springer. v. <2-3>.

95.   Razzaghi, M., *Droplet Size Estimation of 2-Phase Flashing Jets.* Nuclear Engineering and Design, 1989. **114**(1): p. 115-124.

96.   Kitamura, Y., H. Morimitsu, and T. Takahashi, *Critical Superheat for Flashing of Superheated Liquid Jets.* Industrial & Engineering Chemistry Fundamentals, 1986. **25**(2): p. 206-211.

97.   Brown, R. and J.L. York, *Sprays Formed by Flashing Liquid Jets.* AIChE Journal, 1962. **8**(2): p. 149-153.

98.   Reitz, R.D., *A Photographic Study of Flash-Boiling Atomization.* Aerosol Science and Technology, 1990. **12**(3): p. 561-569.

99.   Zhou, Z.F., et al., *An experimental study on the spray and thermal characteristics of R134a two-phase flashing spray.* International Journal of Heat and Mass Transfer, 2012. **55**(15-16): p. 4460-4468.

100.   Brennen, C.E., *Cavitation and bubble dynamics*. Oxford engineering science series1995, New York: Oxford University Press. xv, 282 p.

101.   Oct 3, 2014]; Available from: http://www.edmundoptics.com/optomechanics/apertures/pinholes-slits/precision-pinholes/1794.

102. Tamaki, N., et al., *Effects of cavitation and internal flow on atomization of a liquid jet.* Atomization and Sprays, 1998. **8**(2): p. 179-197.

103. Kundu, P.K., I.M. Cohen, and D.R. Dowling, *Fluid mechanics*. 5th ed2012, Waltham, MA: Academic Press. xxvi, 891 p.

104. Smyth, H.D., E.A. Mejia-Millan, and A.J. Hickey., *The effect of ethanol on solvency, vapor pressure, and emitted droplet size of solution metered dose inhalers containing HFA 134a*, in *Respir Drug Delivery VIII*2002. p. 735-738.

105. Mutair, S. and Y. Ikegami, *On the evaporation of superheated water drops formed by flashing of liquid jets.* International Journal of Thermal Sciences, 2012. **57**: p. 37-44.

106. Yaws, C.L., *Yaws' Critical Property Data for Chemical Engineers and Chemists*, Knovel.

107. Yaws, C.L., *Yaws' Handbook of Thermodynamic and Physical Properties of Chemical Compounds*, Knovel.

108. Design Institute for Physical Properties, S.b.A., *DIPPR Project 801 - Full Version*, Design Institute for Physical Property Research/AIChE.